


Synergistic Pharmacodynamic Effects of Gemcitabine and Fibroblast Growth Factor Receptor Inhibitors on Pancreatic Cancer Cell Cycle Kinetics and Proliferation^[S]

Qingxiang Lin, Zhicheng Qian, William J. Jusko, Donald E. Mager, Wen Wee Ma, and  Robert M. Straubinger

Department of Pharmaceutical Sciences, University at Buffalo, State University of New York, Buffalo, New York (R.M.S.; Z.Q., W.J.J., D.E.M.); Departments of Cell Stress Biology (Q.L., R.M.S.) and Pharmacology and Therapeutics (R.M.S.), Roswell Park Comprehensive Cancer Center, Buffalo, New York; and Department of Medicine, Mayo Clinic, Rochester, Minnesota (W.W.M.)

Received November 10, 2020; accepted March 16, 2021

ABSTRACT

Median survival of pancreatic ductal adenocarcinoma cancer (PDAC) is 6 months, with 9% 5-year survival. Standard-of-care gemcitabine (Gem) provides only modest survival benefits, and combination therapies integrating novel targeted agents could improve outcomes. Fibroblast growth factor (FGF) receptors (FGFRs) play important roles in PDAC growth and invasion. Therefore, FGFR inhibitors (FGFRi) merit further investigation. Efficacy of Gem combined with NVP-BGJ398, a pan-FGFRi, was investigated in multiple PDAC cell lines exposed to the drugs alone and combined. Cell cycle distribution and cell numbers were quantified over time. Two pharmacodynamic models were developed to investigate Gem/BGJ398 interactions quantitatively: a drug-mediated cell proliferation/death model, and a drug-perturbed cell cycle progression model. The models captured temporal changes in cell numbers, cell cycle progression, and cell death during drug exposure. Simultaneous fitting of all data provided reasonable parameter estimates. Therapeutic efficacy was then evaluated in a PDAC mouse model. Compared with Gem alone, combined Gem + FGFRi significantly downregulated ribonucleotide-diphosphate reductase large subunit 1 (RRM1), a gemcitabine resistance (GemR)

biomarker, suggesting the FGFRi inhibited GemR emergence. The cell proliferation/death pharmacodynamic model estimated the drug interaction coefficient $\psi_{death} = 0.798$, suggesting synergistic effects. The mechanism-based cell cycle progression model estimated drug interaction coefficient $\psi_{cycle} = 0.647$, also suggesting synergy. Thus, FGFR inhibition appears to synergize with Gem in PDAC cells and tumors by sensitizing cells to Gem-mediated inhibition of proliferation and cell cycle progression.

SIGNIFICANCE STATEMENT

An integrated approach of quantitative modeling and experimentation was employed to investigate the nature of fibroblast growth factor receptor inhibitor (FGFRi)/gemcitabine (Gem) interaction, and to identify mechanisms by which FGFRi exposure reverses Gem resistance in pancreatic cancer cells. The results show that FGFRi interacts synergistically with Gem to sensitize pancreatic cancer cells and tumors to Gem-mediated inhibition of proliferation and cell cycle progression. Thus, addition of FGFRi to standard-of-care Gem treatment could be a clinically deployable approach to enhance therapeutic benefit to pancreatic cancer patients.

Introduction

Pancreatic ductal adenocarcinoma cancer (PDAC) is the fourth leading cause of cancer-related death in the United States (Siegel et al., 2017) and typically displays a high degree of treatment resistance. Current standard-of-care therapies include gemcitabine (Gem) combined with nab-paclitaxel (Von Hoff et al., 2013) and the FOLFIRINOX combination (Vaccaro et al., 2011). Gem is a difluoro analog of deoxycytidine that targets DNA polymerase and ribonucleotide reductase (Thota et al., 2014). However, it provides only a modest survival benefit (Louvét et al., 2005). Those PDAC patients whose tumors are not intrinsically Gem-resistant (GemR) typically develop GemR and eventually die of unrestrained tumor growth and distant metastasis (Di Marco et al., 2010).

This work was supported by grants from National Institutes of Health National Cancer Institute [Grant R21-CA168454] (to R.M.S. and D.E.M.), [Grant R01-CA198096] (to R.M.S., D.E.M., and W.W.M.), and National Institute of General Medical Sciences [Grant GM131800] (to W.J.J.) and used core resources supported by a National Institutes of Health National Cancer Institute Comprehensive Cancer Center support grant [Grant P30-CA016056] to Roswell Park Comprehensive Cancer Center.

A portion of the work in this publication was presented in preliminary form as a poster at an annual meeting of the American Association for Cancer Research: Abstract 4072: Lin Q, Chaudhuri TR, Straubinger NL, Ma WW, and Straubinger RM (2017) FGFR inhibitors enhance gemcitabine sensitivity in pancreatic ductal adenocarcinoma. Cancer Res July 1, 2017 (77) (13 Supplement) 4072; DOI: 10.1158/1538-7445.AM2017-4072.

<https://doi.org/10.1124/jpet.120.000412>.

^[S] This article has supplemental material available at jpet.aspetjournals.org.

ABBREVIATIONS: AIC, Akaike information criteria; BGJ398, NVP-BGJ398 (infigratinib); ENT1, equilibrative nucleoside transporter 1; FGF, fibroblast growth factor; FGFR, FGF receptor; FGFRi, FGF receptor inhibitor; Gem, gemcitabine; GemR, Gem resistance; hENT1, human equilibrated nucleoside transporter 1; PDAC, pancreatic ductal adenocarcinoma cancer; PI, propidium iodide; RRM1, ribonucleotide reductase large subunit 1.

Integration of novel targeted agents into standard-of-care regimens may improve therapeutic outcomes. The only clinically approved, first-line, molecularly targeted agent in PDAC is erlotinib, an epithelial growth factor (EGF) receptor tyrosine kinase inhibitor that is combined with Gem (Katopodis et al., 2014), but it is seldom used because of its limited benefit. Thus, novel therapies against GemR are needed urgently.

GemR involves both intrinsic and acquired mechanisms. Mechanisms of intrinsic resistance include the preexistence of tumor cells having a drug-resistant, stem-like phenotype (Sarkar et al., 2009) as well as the drug delivery barrier created by tumor microenvironment (Dimou et al., 2012). In contrast, acquired GemR is caused by compensatory, treatment-mediated changes in the activity of proteins that determine drug resistance or sensitivity. For example, overexpression of RRM1 (Nakahira et al., 2007) decreased expression of the primary Gem transporter human equilibrative nucleoside transporter 1 (ENT1) (Greenhalf et al., 2014), and promotion of epithelial-to-mesenchymal transition decreased the efficacy of Gem treatment (Wang et al., 2009). Among these factors, RRM1 is considered one of the most important mechanisms of GemR; its tumor abundance is a biomarker of poorer prognosis and survival of Gem-treated PDAC patients (Jordheim et al., 2011).

Fibroblast growth factor (FGF) receptors (FGFRs) are functionally aberrant in PDAC (Lehnen et al., 2013). Suppression of FGFRs inhibits PDAC growth and invasion (Wagner et al., 1998; Coleman et al., 2014), and FGF/FGFR activity has been implicated as a mechanism of chemo-resistance (Song et al., 2000). FGF/FGFR signaling also promotes epithelial-to-mesenchymal transition, which increases metastatic potential and drug resistance through activation of mitogen-activated protein kinase (MAPK) and signal transducer and activator of transcription (STAT) signaling pathways (Tomlinson et al., 2012; Babina and Turner, 2017). Pharmacological inhibition of FGFR downstream pathways results in improved Gem efficacy (Thoennissen et al., 2009; Vena et al., 2016). Therefore, regulation of these signaling pathways using FGFR inhibitors (FGFRi) may overcome GemR.

A limited number of FGFRi have entered clinical trials, including BGJ398 (NVP-BGJ398, infigratinib) and AZD4547 (Van Cutsem et al., 2017). BGJ398 is a selective pan-FGFRi (Guagnano et al., 2012), which has been investigated in numerous clinical trials for solid tumors having aberrant FGFR activity (Nogova et al., 2017). However, the therapeutic utility of specific FGFRi in PDAC remains unknown. We hypothesize that BGJ398 can sensitize PDAC cells to Gem effects, and that the nature of Gem + BGJ398 interactions could be synergistic (supra-additive). Experimental data were obtained and mathematical models were developed to investigate the mechanisms of Gem + BGJ398 effects upon cell cycle progression and proliferation. A combination regimen based upon insights from the in vitro modeling was designed, and its therapeutic efficacy on PDAC tumor progression was evaluated in a PDAC mouse model.

Materials and Methods

Reagents

Gemcitabine-HCl was obtained from Eli Lilly (Indianapolis, IN) and was prepared as a 1 mM solution in DMSO for in vitro studies

(Sigma-Aldrich, St. Louis, MO). Novartis International AG (Basel, CH) provided BGJ398, which was prepared as a 10 mM solution in DMSO. For in vivo studies, BGJ398 was suspended in acetic acid/acetate buffer pH 4.6/PEG200 1:1, and Gem was dissolved in saline.

Primary antibodies against RRM1 (8637, 1:1000) and β -actin (3700, 1:5000), and secondary anti-rabbit (7074, 1:1000) and anti-mouse (7076, 1:1000) antibodies were from Cell Signaling Technology (Danvers, MA). Primary antibody against ENT1 (sc-377283, 1:1000) was from Santa Cruz Incorporation (Dallas, TX).

Experimental Design

Cell Lines and Culture. The human PDAC cell lines MIAPaCa-2 and PANC-1 were obtained from American Type Culture Collection (Manassas, VA) and cultured in Dulbecco's modified Eagle's medium (Cellgro, Manassas, VA) containing 10% (v/v) fetal bovine serum (Cellgro).

Cell Growth Inhibition by Single Agents. Cells were seeded in six-well plates at $1.5\text{--}2.0 \times 10^5$ cells/well in 2 ml fresh medium, with or without drugs. At this density, vehicle-treated control cells were nearly 100% confluent after 4 days. Cells were treated in triplicate groups with serial dilutions of Gem over a range of 5–75 nM, or to BGJ398 over a range of 1–20 μ M. A concentration of DMSO equivalent to the amount present in the highest-concentration wells was added as a vehicle control. After 72 hours, cells were washed, trypsinized, harvested, counted using a Coulter Counter model Z2 (Beckman Coulter, Hialeah, FL), and the IC₅₀ was determined by fitting with a Hill function, as described below. Cells were subsequently analyzed for cell cycle distribution using flow cytometry, also described below. At least three replicates of experiments were performed.

Cell Growth Inhibition by Combined Agents. Based upon the IC₅₀ data obtained for the single agents, cells were exposed to narrower ranges of drug concentrations, alone and combined. The concentrations chosen for each drug represented the IC₂₅ (concentration mediating 25% inhibition of cell growth), two concentrations flanking the IC₅₀, and the IC₇₅ (concentration mediating 75% inhibition of cell growth). The Gem concentrations used were 6, 7, 7.5, and 15 nM, and for BGJ398 were 1.5, 2.5, 3.0, and 5.0 μ M, yielding 16 pairwise concentrations for combined Gem + BGJ398. Cells were counted at five time points (0, 24, 48, 72, and 96 hours) to obtain temporal dynamic data revealing the onset and time course of drug effects upon rates of cell proliferation and cell cycle progression.

Cell Cycle Analysis. Cell cycle distribution was determined using propidium iodide (PI) DNA staining (Zhou et al., 2015). Cell suspensions in PBS were fixed in 70% cold ethanol and stored at -20°C for a maximum of 1 week. For analysis, the ethanol was removed by centrifugation (220 *g* for 20 minutes at 4°C), washed twice by centrifugation with cold staining buffer (BD Pharmingen, San Diego, CA), and incubated with PI staining buffer containing RNase (BD Pharmingen) for 30 minutes at room temperature in the dark. A FACSCalibur flow cytometer (Becton Dickinson, San Jose, CA) was employed to quantify DNA content based upon PI intensity. The data were analyzed using ModFit LT 4.0 software (Verity Software, Topsham, ME) to determine the fraction of cells in the G0/G1, S, and G2/M phases. The number of cells in each cell cycle phase was derived by multiplying the total number of recovered cells, obtained using a Coulter Counter, by the fraction of cells in each phase, obtained from flow cytometry.

Western Blot Analysis

Cells from the various treatment groups were lysed in cold Radio-immunoprecipitation Assay (RIPA) buffer containing protease and phosphatase inhibitors (Thermo Scientific Inc, MA) and stored on ice. The samples were vortexed three times at 10 minute intervals, and then clarified by centrifugation (220 *g* for 20 minutes, 4°C). The concentration of protein in the supernatant was quantified using a BCA kit (Thermo Scientific). Equal amounts of protein from each sample were loaded on Tris-Bis gradient gels (Invitrogen, Waltham, MA)

and transferred to polyvinylidene fluoride or polyvinylidene difluoride (PVDF) membranes after separation. Membranes were blocked with 5% bovine serum albumin (Fisher Scientific Inc) in PBS containing 0.1% Tween20, incubated with the primary antibody at 4°C overnight (Reagents, above), followed by secondary horseradish peroxidase-conjugated antibody (Santa Cruz Biotechnology Inc, Dallas, TX) for 1 hour. Membranes were developed using an enhanced chemiluminescence substrate kit (Thermo Scientific) and scanned using a ChemiDocMP gel imaging system (Bio-Rad, Hercules, CA).

Model-Based Analysis of Cellular Drug Responses

IC₅₀ determination. The IC₅₀ was determined for both drugs, single and combined, by fitting concentration versus response curves with the inhibitory Hill function:

$$R = R_0 \cdot \left(1 - \frac{I_{\max,d} \cdot C_d^\gamma}{IC_{50,d}^\gamma + C_d^\gamma} \right) \quad (1)$$

where R is the total number of attached cells, R_0 is the cell number in the absence of drug exposure, $I_{\max,d}$ is the maximum growth inhibition, $IC_{50,d}$ is the concentration of half-maximal growth inhibitory effects, γ is the Hill coefficient, and C_d represents the drug concentration, where d represents either Gem or BGJ398.

Analysis of Noncompetitive Drug Interactions at a Single Time Point.

For two-drug interactions, the equation for noncompetitive interactions (Ariens et al., 1957; Chakraborty and Jusko, 2002) is as follows:

$$R = R_0 \cdot \left[1 - \frac{(I_{\max,Gem} \times A + I_{\max,BGJ} \times B + (I_{\max,Gem} + I_{\max,BGJ} - I_{\max,Gem} \times I_{\max,BGJ}) \times A \times B)}{A + B + A \times B + 1} \right] \quad (2)$$

where $A = \frac{C_{Gem}^\gamma}{(\psi \times IC_{50,Gem})^\gamma + C_{Gem}^\gamma}$, $B = \frac{I_{\max,BGJ} \times C_{BGJ}^\gamma}{(IC_{50,BGJ})^\gamma + C_{BGJ}^\gamma}$, R represents the total number of attached cells, R_0 is the cell number at the beginning of drug exposure, $I_{\max,d}$ is the maximum growth inhibition, $IC_{50,d}$ is the concentration of half-maximal growth inhibitory effects, γ_d is the Hill coefficient, and C_d represents the drug concentration, where d represents either Gem or BGJ398.

Based upon experimental data, we hypothesized that BGJ398 could sensitize cells to Gem effects at 72 hours in PDAC cells. The interaction term ψ quantifies the degree to which BGJ398 changed the IC₅₀ of Gem at a single time point. Here, $\psi = 1$ denotes that the effects of the combination are the additive sum of the effect of the drugs as single agents. Therefore, $\psi < 1$ indicates synergism (supra-additivity), and $\psi > 1$ indicates antagonism (Pawaskar et al., 2013). The ψ term was estimated after fixing the parameters that were estimated using (eq. 1).

Basic Cell Proliferation/Death Model.

The basic cell proliferation/death model is shown in Fig. 1. The same equations for cell growth inhibition were used for BGJ398 and Gem. Unperturbed cell growth (without drug) was described with a logistic growth function (Zhu et al., 2015; Miao et al., 2016a,b):

$$\frac{dR}{dt} = k_g \cdot R \cdot \left(1 - \frac{R}{R_{ss}} \right); \quad R(0) = R_0 \quad (3)$$

where R is the cell number at time t , k_g is the first-order growth rate constant, R_{ss} is the cell number measured at steady-state, and R_0 is the initial cell number at time zero. The function $(1 - \frac{R}{R_{ss}})$ represents cell proliferation restrained by cell contact inhibition in a logistic manner. The concentrations of Gem or BGJ398 were assumed to be constant over the exposure periods.

Four transit compartments were employed in the model to describe the delay in the drug signal, which ultimately transitions cells out of the

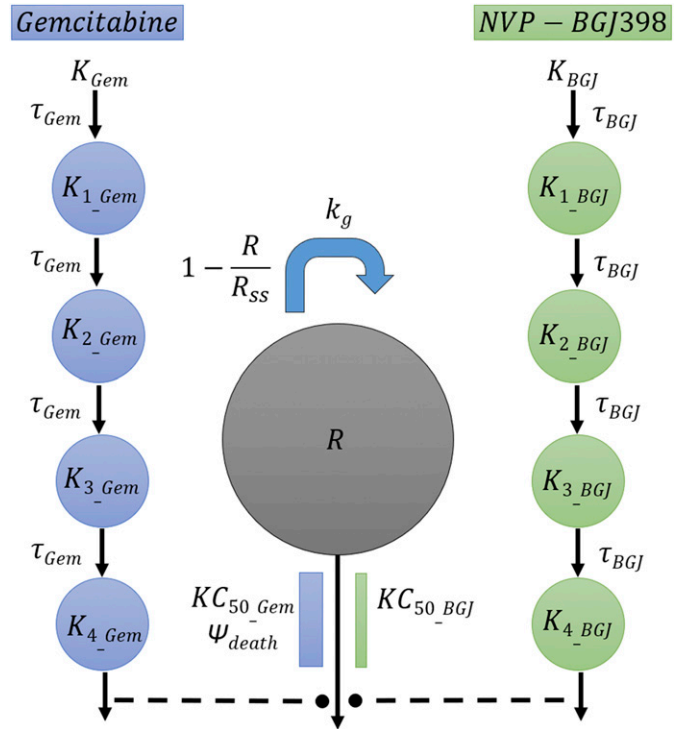


Fig. 1. Schematic of the basic cell proliferation/death pharmacodynamic model to assess interactions between gemcitabine and BGJ398. Proposed pharmacodynamic model representing the effects of Gem and BGJ398, alone and combined, on cell proliferation and death. Cell number is represented by R and cells proliferate with rate constant k_g . $KC_{50,Gem}$ and $KC_{50,BGJ}$ are the drug concentrations at which half-maximum cell loss effects were achieved for Gem and BGJ398. The $1 - \frac{R}{R_{ss}}$ function restrains cell proliferation because of contact inhibition in a logistic manner. Four transit compartments (mean transit time = τ) describe the delayed effects of BGJ398 and Gem on cell death. The open rectangles represent the stimulation of cell death by BGJ398 and Gem. The ψ_{death} is a drug interaction parameter that quantifies the degree to which BGJ398 changes the IC₅₀ of Gem. Other parameters are described in Tables 2 and 3.

viable, cycling population (Ait-Oudhia et al., 2013). The differential equations for drug-mediated inhibition of cell proliferation or killing are:

$$K_d = \frac{K_{\max,d} \cdot C_d^{\gamma_k}}{KC_{50,d}^{\gamma_k} + C_d^{\gamma_k}} \quad (4)$$

$$\frac{dK_1}{dt} = \frac{1}{\tau_d} \cdot (K_d - K_1); \quad K_1(0) = 0 \quad (5)$$

$$\frac{dK_j}{dt} = \frac{1}{\tau_d} \cdot (K_{j-1} - K_j); \quad K_j(0) = 0 \quad (6)$$

$$\frac{dR}{dt} = k_g \cdot R \cdot \left(1 - \frac{R}{R_{ss}} \right) - K_4 \cdot R; \quad R(0) = R_0 \quad (7)$$

where K_d is the Hill equation of cell loss by killing or growth inhibition for drug d . $K_{\max,d}$ represents the maximum cell loss rate for drug d , $KC_{50,d}$ is the drug concentration at which half-maximum cell loss effects were achieved, γ_k represents the Hill coefficient that modifies the shape of the concentration-response curve, and C_d is the concentration of drug d in the medium. In the differential equations for the transit compartments, K_i is the input function for the inhibitory drug signal, and τ_d is the mean transit time of the drug signal K_j through each of the successive compartments, where j represents compartments 2–4. Four transit compartments were optimal based upon comparison of the Akaike information criteria (AIC) for variations on the model (Zhu et al., 2015; Miao et al., 2016b; Molins and Jusko, 2018).

The basic model makes the simplifying assumption that the cytoplasmic concentrations of the drugs were equal to the extracellular concentrations in the medium. ENT1 is the major drug transporter of Gem (Rauchwerger et al., 2000; Binenbaum et al., 2015; Namba et al., 2015), and the capacity of cells to equilibrate extracellular and intracellular Gem concentrations would be reflected by ENT1 abundance and self-regulation. Quantification of intracellular concentrations of dFdCTP, the active form of Gem that is incorporated into DNA, causing cell cycle arrest (Battaglia and Parker, 2011), was not performed, and integrating the dynamics of dFdCTP is left as a future mechanistic extension of the model.

We hypothesized that BGJ398 could sensitize cells to Gem effects by downregulation of key effectors of GemR. The interaction term ψ_{death} was employed to describe drug interactions affecting cell growth or killing that are not captured in the structured models; ψ_{death} quantifies the degree to which BGJ398 changed the IC_{50} of Gem. As above, $\psi_{death} = 1$ denotes additive of interaction, $\psi_{death} < 1$ indicates synergism (supra-additivity), and $\psi_{death} > 1$ indicates antagonism.

For the effect of the combined drugs, eqs. 4 and 7 were rewritten as:

$$K_{Gem_comb} = \frac{K_{max_Gem} \cdot C_{Gem}^{\gamma_{Gem}}}{(\psi_{death} \cdot KC_{50_Gem})^{\gamma_{Gem}} + C_{Gem}^{\gamma_{Gem}}} \quad (8)$$

$$\frac{dR}{dt} = k_g \cdot R \cdot \left(1 - \frac{R}{R_{ss}}\right) - (K_{4_BGJ} + K_{4_Gem}) \cdot R; \quad R(0) = R_0 \quad (9)$$

Mechanism-Based Pharmacodynamic Models

Basic Cell Cycle Model. Flow cytometry analysis was employed to assess the fractional cell cycle distribution based on cellular DNA content (Hamed et al., 2013; Zhu et al., 2015; Miao et al., 2016a). Cell distribution in G_0/G_1 , S, and G_2/M phases was described as follows:

$$\frac{dG_1}{dt} = 2 \cdot k_{G2G1} \cdot \left(1 - \frac{R_{total}}{R_{ss}}\right) - k_{G1S} \cdot CTI_2^{\gamma} \cdot G_1; \quad G_1(0) = G_{10} \quad (10)$$

$$\frac{dS}{dt} = k_{G1S} \cdot CTI_2^{\gamma} \cdot G_1 - k_{SG2} \cdot S; \quad S(0) = S_0 \quad (11)$$

$$\frac{dG_2}{dt} = k_{SG2} \cdot S - k_{G2G1} \cdot G_2; \quad G_2(0) = G_{20} \quad (12)$$

The total number of cells in each cell cycle compartment was calculated by multiplying the number of cells (R_{total}) in each sample by the fraction of cells in each cycle phase (f_{G1} , f_S , and f_{G2}), where G_1 is the G_0/G_1 phase cell number, S is the S phase cell number, and G_2 is the G_2/M phase cell number.

In the absence of drug, proliferating cells transition through consecutive cycle phases with first-order rate constants k_{G1S} , k_{SG2} , and k_{G2G1} that represent the cell cycle transitions through G_0/G_1 , S, and G_2/M phases. Cell proliferation was assumed to slow as cells approached confluence, which was implemented as a reduction in the transit rate from G_0/G_1 phase to S phase (Wu et al., 1996) and is represented by the contact inhibition term I_2 between the G_0/G_1 and S phases:

$$I_2 = \frac{I_{max_CTI} \times T^{\gamma_{CTI}}}{IT_{50}^{\gamma_{CTI}} + T^{\gamma_{CTI}}} \quad (13)$$

The delayed effects of contact inhibition were implemented with a feedback function (Karlsson et al., 2005), where CTI_1 and CTI_2 represent two signal transduction compartments (CTI_1 and CTI_2):

$$\frac{dCTI_1}{dt} = k_t \cdot \left(\frac{S}{S_0}\right) - k_t \cdot CTI_1; \quad CTI_1 = 1 \quad (14)$$

$$\frac{dCTI_2}{dt} = k_t \cdot (CTI_1 - CTI_2); \quad CTI_2 = 1 \quad (15)$$

where I_{max_CTI} is the maximum cell contact inhibition, T represents the time after cell seeding, IT_{50} is the time to half-maximal inhibition, γ_{CTI} is the Hill coefficient, and k_t is the first-order transit rate constant

between the two CTI compartments. $I_{max_CTI} = 1.0$ (complete inhibition of proliferation was assumed).

Modeling BGJ398 Effects on Cell Cycle. Cell cycle data suggested that BGJ398 inhibits the cell cycle transition from G_0/G_1 to S and from G_2/M to G_0/G_1 phase, and the inhibition functions for both transitions were the same:

$$Inh_{BGJ} = \frac{I_{max_BGJ} \cdot C_{BGJ}^{\gamma_{BGJ}}}{IC_{50_BGJ}^{\gamma_{BGJ}} + C_{BGJ}^{\gamma_{BGJ}}} \quad (16)$$

where Inh_{BGJ} is the inhibition term for the two cell cycle transitions mediated by BGJ398, I_{max_BGJ} is the maximal BGJ398-mediated cell cycle arrest, IC_{50_BGJ} is the concentration of BGJ398 mediating half-maximal cell cycle arrest effects, C_{BGJ} represents the concentration of BGJ398, and γ_{BGJ} is the Hill coefficient of BGJ398-mediated cell cycle arrest. For the sake of parsimony, we assumed that the inhibitory Hill function was the same for G_0/G_1 and G_2/M phases, and that the maximum effect of G_0/G_1 and G_2/M cell cycle accumulation (I_{max_BGJ}) was fixed to 1.0.

In the presence of BGJ398, the cell cycle distribution in each compartment was defined as:

$$\frac{dG_{1_BGJ}}{dt} = 2 \cdot k_{G2G1} \cdot \left(1 - \frac{R_{total}}{R_{ss}}\right) \cdot (1 - Inh_{BGJ}) - k_{G1S} \cdot CTI_2^{\gamma} \cdot G_1 \cdot (1 - Inh_{BGJ}); \quad G_1(0) = G_{10} \quad (17)$$

$$\frac{dS_{BGJ}}{dt} = k_{G1S} \cdot CTI_2^{\gamma} \cdot G_1 \cdot (1 - Inh_{BGJ}) - k_{SG2} \cdot S; \quad S(0) = S_0 \quad (18)$$

$$\frac{dG_{2_BGJ}}{dt} = k_{SG2} \cdot S - k_{G2G1} \cdot G_2 \cdot (1 - Inh_{BGJ}); \quad G_2(0) = G_{20} \quad (19)$$

Modeling Gem Effects on Cell Cycle. As reported previously (Cappella et al., 2001; Zhu et al., 2015), transient arrest in S phase was observed when MIAPaCa-2 cells were treated with concentrations of Gem relevant to its IC_{50} . Analogous to the model for cell response to BGJ398, a Hill function was used to describe the initial effect of Gem on the S- G_2/M phase transition:

$$Inh_{Gem_SG2} = \frac{I_{max_Gem} \cdot C_{Gem}^{\gamma_{Gem}}}{IC_{50_Gem}^{\gamma_{Gem}} + C_{Gem}^{\gamma_{Gem}}} \quad (20)$$

The differential equations describing cell cycle distribution after Gem exposure are:

$$\frac{dG_{1_Gem}}{dt} = 2 \cdot k_{G2G1} \cdot \left(1 - \frac{R_{total}}{R_{ss}}\right) - k_{G1S} \cdot CTI_2^{\gamma} \cdot G_1; \quad G_1(0) = G_{10} \quad (21)$$

$$\frac{dS_{Gem}}{dt} = k_{G1S} \cdot CTI_2^{\gamma} \cdot G_1 - k_{SG2} \cdot S \cdot (1 - Inh_{Gem_SG2}); \quad S(0) = S_0 \quad (22)$$

$$\frac{dG_{2_Gem}}{dt} = k_{SG2} \cdot S \cdot (1 - Inh_{Gem_SG2}) - k_{G2G1} \cdot G_2; \quad G_2(0) = G_{20} \quad (23)$$

The initial, transient S-phase arrest mediated by Gem activates compensatory changes in GemR proteins, such as upregulation of RRM1 and DNA excision repair proteins (Binenbaum et al., 2015), and after a time lag, cell cycle progression resumes. As described previously (Zhu et al., 2015), a delay in the emergence of GemR, T_{Rlag_Gem} , was implemented, and growth inhibition by Gem was described as:

$$Inh_{Gem_SG2} = \frac{I_{max_Gem} \cdot C_{Gem}^{\gamma_{Gem}}}{IC_{50_Gem}^{\gamma_{Gem}} + C_{Gem}^{\gamma_{Gem}}}; \quad \text{if } T \leq T_{Rlag_Gem} \quad (24)$$

where T_{Rlag_Gem} is assumed to be linearly proportional to the logarithm of Gem concentrations:

$$T_{Rlag_Gem} = k_{Rlag_Gem} \cdot \log_{10}(C_{Gem}) \quad (25)$$

where k_{Rlag_Gem} is a linear rate constant for the delay in Gem-induced resistance.

$$Inh_{Gem_SG2} = \frac{I_{max_Gem} \cdot C_{Gem}^{\gamma_{Gem}}}{IC_{50_Gem}^{\gamma_{Gem}} + C_{Gem}^{\gamma_{Gem}}} \cdot \exp(-k_{R_Gem} \cdot (t - T_{Rlag_Gem}));$$

if $T > T_{Rlag_Gem}$ (26)

where k_{R_Gem} is a first-order rate constant used to characterize the rate of recovery to normal cell cycle progression.

Modeling Combined Drug Effects on Cell Cycle. The combination of Gem and BGJ398 was assumed to act on cell cycle distribution by the same mechanisms as they do as single agents. However, based upon experimental data, BGJ398 was also assumed to sensitize cells to Gem by increasing T_{Rlag_Gem} , the onset of GemR, as well as decreasing the magnitude of GemR:

$$T_{Rlag_comb} = k_{Rlag_Gem} \cdot \log_{10}(C_{Gem}) \cdot (1 + k_{comb1} \cdot C_{BGJ}) \quad (27)$$

$$k_{R_comb} = k_{R_Gem} \cdot (1 - k_{comb2} \cdot C_{BGJ}) \quad (28)$$

where T_{Rlag_comb} is the delay in GemR when combined with BGJ398, and k_{comb1} and k_{comb2} are linear coefficients for the prolonged delay in, and reduced magnitude of, GemR mediated by BGJ398.

Finally, the drug interaction term ψ_{cycle} was multiplied by the IC_{50} of Gem to quantify other mechanisms by which BGJ398 affects the Gem IC_{50} . The resulting equations are:

$$Inh_{Gem_SG2_comb} = \frac{I_{max_Gem} \cdot C_{Gem}^{\gamma_{Gem}}}{(\psi_{cycle} \cdot IC_{50_Gem})^{\gamma_{Gem}} + C_{Gem}^{\gamma_{Gem}}}; \quad \text{if } T \leq T_{Rlag_comb} \quad (29)$$

$$Inh_{Gem_SG2_comb} = \frac{I_{max_Gem} \cdot C_{Gem}^{\gamma_{Gem}}}{(\psi_{cycle} \cdot IC_{50_Gem})^{\gamma_{Gem}} + C_{Gem}^{\gamma_{Gem}}} \cdot \exp(-k_{R_Gem} \cdot (1 - k_{R_comb2} \cdot C_{BGJ}) \cdot (t - T_{Rlag_comb})); \quad \text{if } T > T_{Rlag_comb} \quad (30)$$

Data Analysis and Computation. ADAPT5 (Biomedical Simulations Resource, University of South California, Los Angeles) was used to fit the data using a naïve-pooled approach, and parameters were estimated using the maximum likelihood algorithm. The ADAPT5 computational code is available in the *Appendix* section. The variance model was:

$$V_i = (\sigma_1 + \sigma_2 \cdot Y(t_i))^2 \quad (31)$$

where V_i is the variance of the drug response at the i^{th} time point (t_i), and $Y(t_i)$ is the predicted response at i^{th} time point. The variance parameters σ_1 and σ_2 were estimated. The goodness-of-fit was analyzed using visual inspection of model fitting, goodness-of-fit criteria, the sum of squared residuals, the AIC, and the CV% of the estimated parameters.

Animal Studies

All procedures involving animals were approved in advance by the Institutional Animal Care and Use Committees of the Roswell Park

Comprehensive Cancer Center (Buffalo, NY) and the University at Buffalo, State University of New York.

Donor Tumor Implantation. Five million MIA PaCa-2 cells in cold diluted 1:1 Matrigel (Corning): sterile PBS were injected subcutaneously in the upper abdominal area of 6- to 8-week-old male C.B-Igh-1^b/IcrTac-Prkdc^{scid} mice. When tumors reached 1000 mm³, the donor tumors were harvested rapidly after euthanasia, immersed in ice-cold RPMI-1640 (Cellgro), and cut into 2 × 2 × 2 mm³ fragments under sterile conditions. The fragments were then implanted subcutaneously through a small incision under the abdominal skin under isoflurane anesthesia.

Analysis of Treatment Efficacy. When the tumor volume reached 150–200 mm³, mice were randomized, allocated into treatment groups ($n = 5/\text{group}$) of equivalent mean volumes, and treated with the regimens indicated. Gem was administered intraperitoneally twice weekly (day 0, 3), and BGJ398 was dosed orally by gavage for 5 days, beginning on day 0, the first day of Gem treatment. A 2-day treatment holiday was imposed before the next weekly cycle. Tumor volume and body weight were measured 2 to 3 times weekly using a caliper, and volume was calculated as: volume = length × width × height × 0.5. When tumor reached the protocol volume limit of 2000 mm³, or any dimension reached 20 mm, mice were removed from study. Survival was recorded as the time to this protocol volume limit. When more than 60% of the mice in the vehicle, Gem, and BGJ398 groups had been removed from study because of tumor progression (day 21), the experiment was terminated.

Data and Statistical Analysis

The data and statistical analysis comply with recommendations on experimental design and analysis in pharmacology (Curtis et al., 2018). Experimental data are reported as means ± SD as indicated in specific figures and tables. Individual cell count data are shown in the model fittings (Figs. 2, 4 and 5). Details of data analysis by computational modeling is described in *Materials and Methods*. The time of tumor progression to a volume limit of 2000 mm³ was assessed using Kaplan-Meier analysis, and group-wise comparisons were analyzed by two-sided unpaired Student's t test. P values <0.05 were considered statistically significant.

Results

Analysis and Modeling of Single and Combined Drug Effects on Cell Proliferation and Death. Cells were seeded in the presence of various concentrations of Gem or BGJ398, and the IC_{50} of each was calculated after 3 days of incubation. The IC_{50} of Gem on MIA PaCa-2 cells was 8.28 nM, and its I_{max} was 0.954. The IC_{50} of BGJ398 was 2.80 μM, and its I_{max} was 1.0. The basic cell growth model of Fig. 1 captured well the observed effects of both drugs on MIA PaCa-2 cell proliferation (Fig. 2), which are shown along with the model fits. Model parameter estimates are in

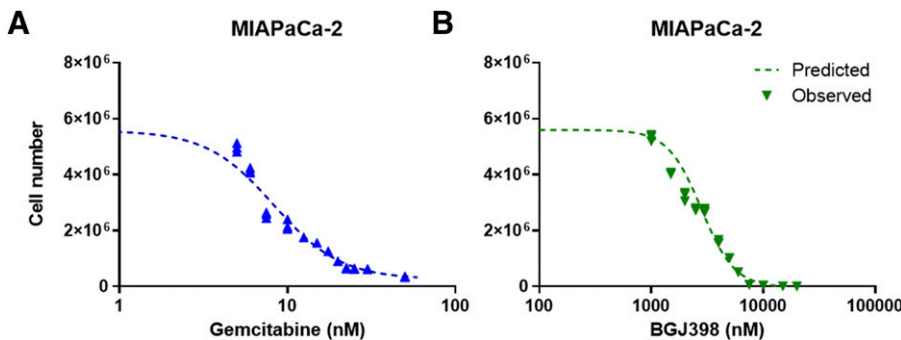


Fig. 2. Concentration-dependence of cell proliferation responses to gemcitabine and BGJ398 exposure. MIA PaCa-2 cells were exposed to the indicated concentrations of (A) gemcitabine (5–75 nM) and (B) BGJ398 (1–20 μM) for 3 days, at which time cells were detached and counted. Symbols are observed experimental cell counts, and dotted lines depict curves generated by fitting cell count data using the inhibitory Hill function.

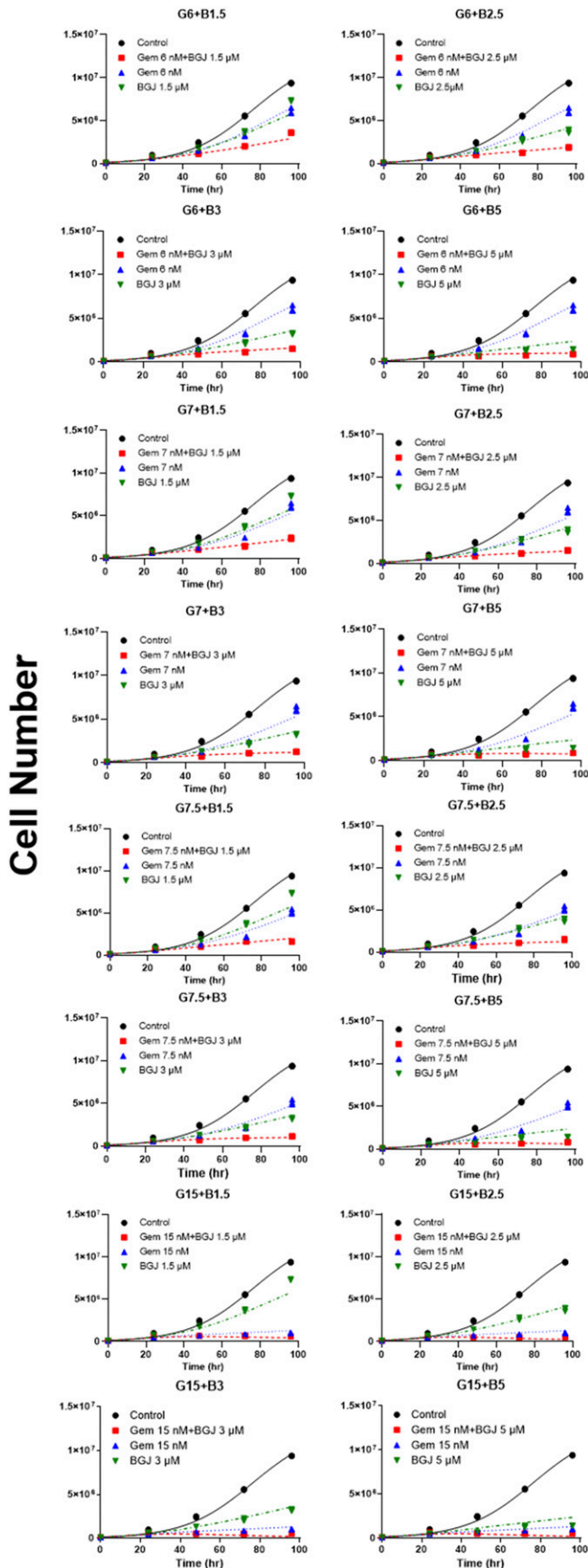


Fig. 3. Effects of gemcitabine and BGJ398, alone and combined, on MIAPaCa-2 cell proliferation. MIAPaCa-2 cells were exposed to vehicle

Table 1. Concentration-response curves were also obtained for PANC-1 cells (Supplemental Figs. 1, A and B). The IC_{50} of Gem was 8.06 nM, and its I_{max} was 0.726, whereas the IC_{50} of BGJ398 was 10.4 μ M, and its I_{max} was 0.98 (Supplemental Table 1). These estimated IC_{50} values helped define the appropriate concentration ranges for subsequent experiments.

Based upon the IC_{50} data obtained, MIAPaCa-2 cells were exposed to ranges of concentrations of Gem and BGJ398, alone and in 16 pairwise concentrations. The cells were counted at multiple time points over 96 hours to obtain data for drug effects upon rates of cell proliferation (Fig. 3). The data were fitted with the pharmacodynamic cell growth/death model of Fig. 1. Table 2 shows the parameter estimates obtained, which were reasonable. Cell proliferation over time was fitted using a logistic growth function. The estimated rate constant of unperturbed MIAPaCa-2 cell growth (k_g) was 0.059 $hour^{-1}$. The cell line approached a steady-state after 96 hours, at which time the estimated cell number was 1.25×10^7 . The doubling time for MIAPaCa-2 cells, calculated as $\ln(2) k_g^{-1}$, was 11.7 hours.

For activity, Gem must be transported into cells and then transformed metabolically into its triphosphate metabolite, dFdCTP (Plunkett et al., 1995; Battaglia and Parker, 2011). Therefore, the model of Fig. 1 included a time-dependent signal transduction component to describe the delay in Gem cytostatic and cytotoxic effects. Four transit compartments appeared to be optimal, based upon comparisons of the AIC for variations on the model. With this feature, the developed model captured well the temporal effects of Gem and BGJ398 on MIAPaCa-2 cells as both single and combined agents (Fig. 3; Table 2). The mean transit time of drug signal propagation was calculated as $MTT = N \cdot \tau_k$, where N is the number of transit compartments, and τ_k is the mean signal transduction time for drug k . The calculated mean transit times were 35.1 hours for BGJ398 and 26.5 hours for Gem. The estimated maximal cell killing constants ($hour^{-1}$) for Gem and BGJ398 were 0.054 $hour^{-1}$ and 0.058 $hour^{-1}$. The IC_{50} values for cell killing effects (KC_{50_Gem} and KC_{50_BGJ}) were estimated as 9.15 nM for Gem and 3.08 μ M for BGJ398.

To investigate the mechanisms and nature of BGJ398 interactions with Gem, the drug interaction parameter ψ_{death} was introduced on the IC_{50} term of Gem (Fig. 1). Its fitted value (Table 2) was 0.798 (CI 0.706–0.890), where $\psi_{death} = 1$ represents pure additivity of interaction, suggesting that the combination of Gem + BGJ398 exhibits modest synergism on MIAPaCa-2 cells. Effects of the single-agent- and combined drugs were also investigated in PANC-1 cells at 72 hours (Supplemental Fig. 1C). Analysis of two-drug interactions (eq. 2) estimated ψ as 0.698 (CI 0.437–0.958) (Supplemental Table 1) for combined Gem + BGJ398 on PANC-1 cells, suggesting synergistic drug interactions on this second PDAC cell line.

(black), the indicated concentrations of Gem (6, 7, 7.5, 15 nM, blue) or BGJ398 (1.5, 2.5, 3, 5 μ M, green) alone, or to 16 pairs of the combined drugs at the indicated concentrations (red) over 0–96 hours ($n = 3$). At the time points indicated, cells were counted, and the data for the drugs, alone and combined, were fit simultaneously to the cell proliferation/death model of Fig. 1. Symbols are the observed data, and model fits are represented by lines. The drug-drug interaction parameters, including ψ_{death} were estimated by simultaneous fitting of all data using ADAPT5 software. In all panels, B represents the BGJ398 concentration in micromolar, and G represents the Gem concentration in nanomolar.

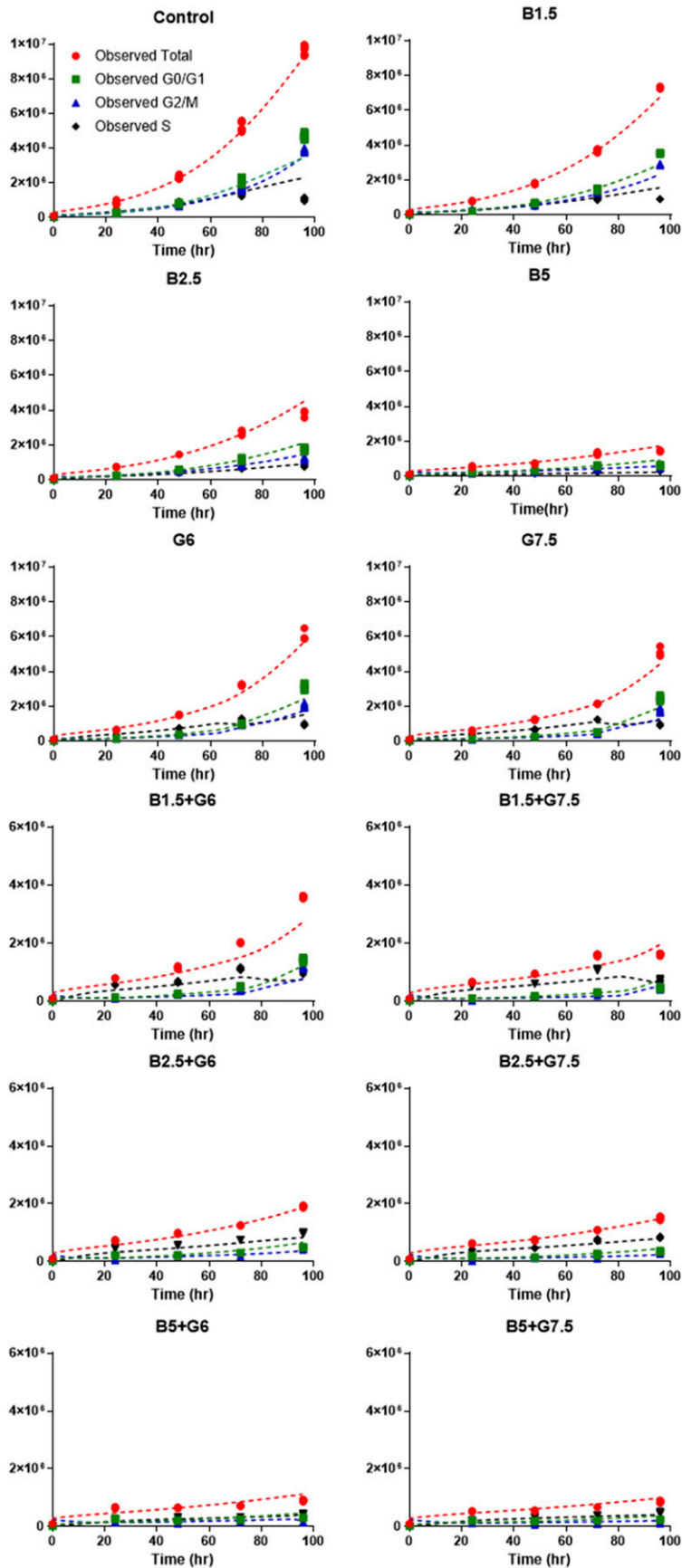


Fig. 4. Effects of gemcitabine and BGJ398, alone and in combination, on cell cycle kinetics. MIAPaCa-2 cells were exposed to Gem (6, 7, 7.5 nM) or BGJ398 (1.5, 2.5, 5 μ M) alone, or to nine pairs of drug concentrations over 0–96 hours, as described in *Materials and Methods*, and analyzed for cell cycle distribution by flow cytometry ($n = 9$), based upon propidium iodide DNA staining. Cell cycle population is indicated for G0/G1 (green), S (blue), and G2/M (black) phases. Symbols represent observed cell number data for total cells (red) or cell number in each cycle phase. Lines depict simultaneous fitting of all data to the cell cycle kinetics models of Figs. 5 and 6. The drug-drug interaction parameters of the model, including ψ_{cycle} , were estimated by simultaneous fitting of all data using ADAPT5 software. In all panels, B indicates BGJ398 concentration in micromolar, and G indicates Gem concentration in nanomolar.

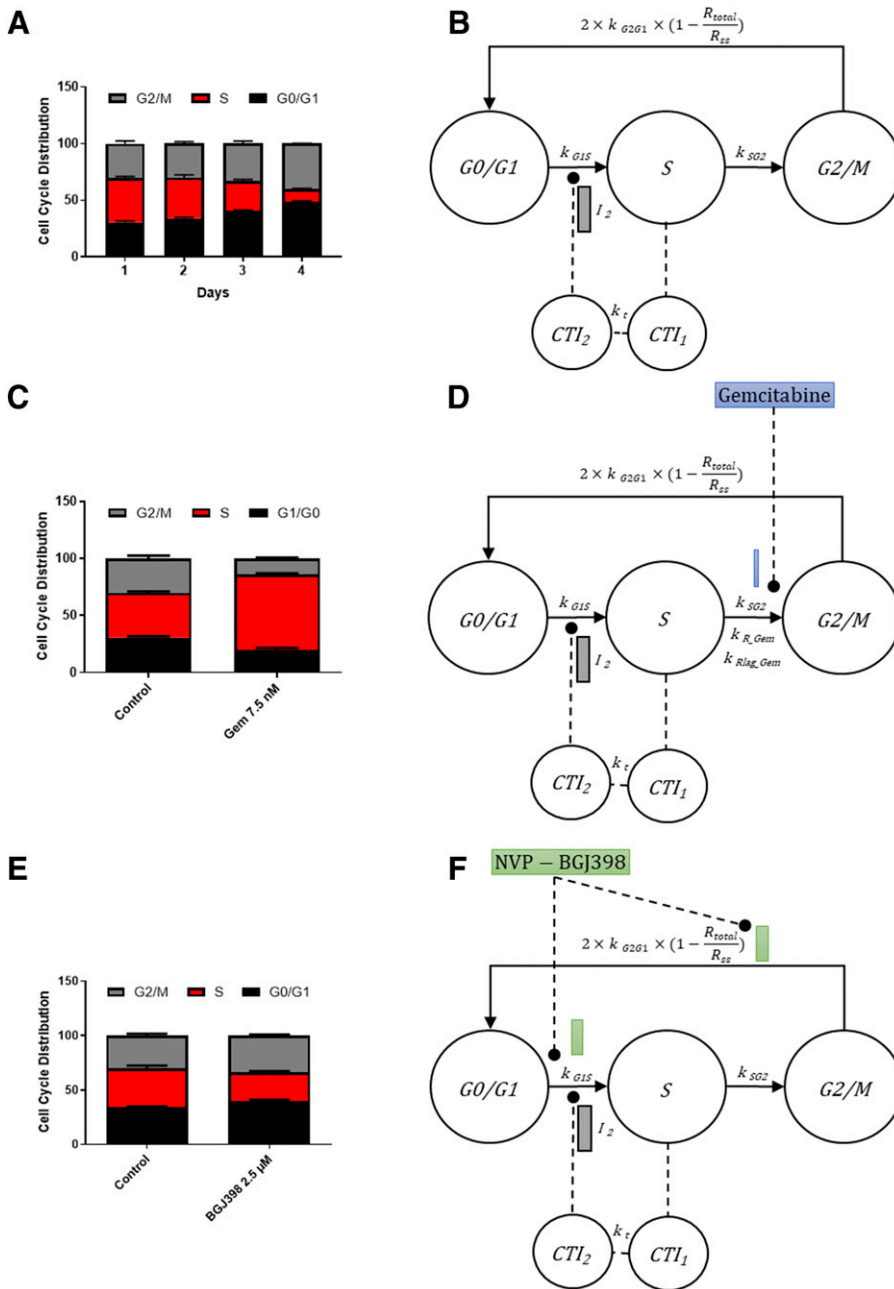


Fig. 5. Model schematics and effects of gemcitabine and BGJ398 analyzed using cell cycle progression pharmacodynamic model. (A) Representative fraction of MIAPaCa-2 cells in each cell cycle phase in vehicle control group over 4 days ($n = 9$). Cell cycle distribution was analyzed by flow cytometry, based upon propidium iodide DNA staining. (B) Schematic of the mechanism-based cell cycle model for the unperturbed vehicle control. The circles labeled with G0/G1, S, and G2/M represent cell numbers in each cell cycle phase. Rate constants for transition from G0/G1 to S and to G2/M phases are represented by k_{G1S} , k_{SG2} , and k_{G2G1} . The $2 \cdot R - \frac{R}{R_{ss}}$ function depicts cell proliferation and the effect of contact inhibition, and the CTI₁ and CTI₂ compartments reflect the delayed contact inhibition effects. The reduction in the transit rate from G0/G1 phase to S phase by contact inhibition effects is represented by I_2 , and k_t is the first-order transit rate constant between the two CTI compartments. (C) Representative fraction of cells in each cell cycle phase during Gem exposure (7.5 nM) of MIAPaCa-2 cells for 48 hours. (D) Schematic of the mechanism-based cell cycle model for Gem. Inhibition term of cell cycle transition from S to G2/M phase by Gem is depicted using a blue bar. $k_{R_{Gem}}$ is a linear rate constant for the delay in Gem-induced resistance. $k_{R_{lag_{Gem}}}$ is a first-order rate constant characterizing the rate of recovery to regular cell cycle progression. (E) Representative fractions of cells in each cell cycle phase during BGJ398 exposure (2.5 μM) of MIAPaCa-2 cells for 48 hours. (F) Schematic of the mechanism-based cell cycle model for BGJ398. Term for inhibition of cell cycle transition from G0/G1 to S phase and from G2/M to G0/G1 phase by BGJ398 is depicted using green bars. Data shown are mean \pm S.D.

Analysis and Modeling of Single and Combined Drug Effects on Cell Cycle Distribution and Progression.

Gemcitabine alters cell cycle progression mechanistically. Therefore, we employed flow cytometry to acquire data on cell cycle progression and distribution. Fig. 4 shows cell cycle distribution over time for unperturbed (control) MIAPaCa-2 cells and for cells treated for up to 96 hours with Gem and BGJ398 as single agents or combined. As total cell number increased in control cells, there was a gradual reduction in S-phase cells as the cultures underwent increasing contact inhibition (Fig. 4). Both Gem and BGJ398 reduced the total number of cells over time, alone and in combination.

To analyze the drug-mediated changes in cell cycle within a quantitative, pharmacologically based framework, a series of pharmacodynamic cell cycle structural models were developed for analysis of unperturbed and drug-treated cells.

Such models have been used to characterize the responses of cancer cells to combination chemotherapy agents and generate experimentally testable hypotheses as to underlying mechanisms (Hamed et al., 2013; Niu et al., 2019). Fig. 5 shows the structural models for cell cycle progression for unperturbed control cells and cells treated with single-agent Gem and BGJ398. Fig. 6 shows the final model, to which the cell cycle distribution data of Fig. 4 were fitted simultaneously, providing the parameter estimates shown in Table 3.

In unperturbed cells, the fraction of cells in G0/G1 phase increased significantly over 4 days, and the fraction of cells in S phase decreased as contact inhibition and depletion of nutrients reduced cell proliferation rates (Fig. 5A). Therefore, unperturbed growth was modeled as a time-delayed suppression of the G0/G1-S transition, resulting in an accumulation of G0/G1-phase cells (Fig. 5B). Mechanistically, this

TABLE 1
Parameter estimates for each drug after 72-hour treatment of MIAPaCa-2 cells

Parameter (Units)	Definition	Estimate	CV%
R_0 (1×10^6 cell)	Cell counts in vehicle group on day 3	5.56	6.5
I_{max_Gem}	Maximal inhibitory effects of gemcitabine	0.954	0.9
IC_{50_Gem} (nM)	IC_{50} of gemcitabine	8.29	7.3
γ_{Gem}	Hill coefficient for gemcitabine	2.18	7.5
I_{max_BGJ}	Maximal inhibitory effects of BGJ398	1.00	0.2
IC_{50_BGJ} (μ M)	IC_{50} of BGJ398	2.80	13.3
γ_{BGJ}	Hill coefficient for BGJ398	2.82	10.9

shift in distribution results from activation of cell cycle checkpoints (Wu et al., 1996). The cell cycle pharmacodynamic model fitted the control data well with reasonable estimates (Fig. 4; Table 3). The approximate doubling time (T_{double}) of MIAPaCa-2 cells, calculated as $T_{double} = k_{G1S}^{-1} + k_{SG2}^{-1} + k_{G2G1}^{-1}$, was 17.9 hours, which is close to a previous modeling estimate of T_{double} for MIAPaCa-2 cells (Miao et al., 2016b). The cell number at steady-state (R_{ss}) was 1.58×10^7 per well for 6-well plates. The time at which half-maximal cell contact inhibition (IT_{50}) was achieved was estimated as 56.6 hours, approximately half of the 120 hours required to reach 100% confluency. Overall, the values estimated by the model are in concordance with experimental observations.

With Gem treatment, cells initially accumulated in S phase in a time- and concentration-dependent manner (Fig. 5C; Supplemental Fig. 2) according to the rate constant k_{SG2} , but S-phase progression eventually resumed, and the cell cycle distribution resembled that of the unperturbed control group by day 4 (Supplemental Fig. 2). The approach to modeling Gem effects is shown in Fig. 5D. The model assumes that recovery from cell cycle arrest is the result of the emergence of GemR mechanisms, rather than from drug loss from the medium, and the lag time function (T_{Rlag_Gem}) is assumed to be proportional to the log of the Gem concentration (eq. 25). Data for the cell cycle effects of Gem concentrations ≥ 15 nM were not incorporated into the model because the mechanisms of Gem action at higher concentrations are complex. For example, 15 nM Gem induced aneuploidy, which was followed by marked sub-G₁ apoptosis (Supplemental Fig. 3). However, with Gem concentrations near the IC_{50} , neither aneuploidy nor apoptosis were detected. The model characterized the cell cycle data well (Fig. 4). The estimated lag time for GemR emergence was approximately 61–69 hours (Supplemental Table 2), and the estimated parameters associated with GemR (k_{R_Gem} and k_{Rlag_Gem}) suggested that continuous Gem exposure resulted in the emergence of GemR (Table 3).

Treatment with BGJ398 induced G₀/G₁ and G₂/M phase cell cycle arrest (Fig. 5E), which is consistent with results for some growth factor receptor tyrosine kinase inhibitors (Zhu et al., 2001; Strömberg et al., 2006). The effects of BGJ398 were modeled as shown in Fig. 5F. The cycle phase transition rate constants for G₀/G₁ to S phase (k_{G1S}) and for G₂/M to G₀/G₁ phase (k_{G2G1}) were both multiplied by inhibition terms, and the model fitted the cell cycle effects of BGJ398 treatment well, with reasonable parameter estimates (Fig. 4; Table 3). The estimated IC_{50} of BGJ398 effects on cell cycle progression was close to the overall IC_{50} for cell growth inhibition, which suggested that delay of cell cycle progression is the major mechanism of cell growth inhibition mediated by BGJ398.

The cell cycle effects of treatment with combined Gem + BGJ398 differed markedly from those of Gem alone. Treatment with Gem alone mediated S-phase arrest that persisted over 3 days of exposure (Fig. 5D), and cycling resumed by day 4 as resistance mechanisms emerged (Supplemental Fig. 3). In contrast, treatment with combined Gem + BGJ398 mediated prolonged S-phase arrest that was observed by day 3 and persisted through day 4 (Figs. 6, A and B), suggesting that BGJ398 can augment Gem effects on S-phase arrest and postpone the onset of GemR. Consistent with the model developed for Gem effects (Fig. 5D), in which continuing Gem exposure eventually upregulates GemR factors, western blot analysis showed that, compared with vehicle control cells, Gem alone downregulated RRM1, a key mediator of GemR, after 24 hours (Fig. 6C). After 72 hours of exposure, Gem upregulated RRM1 expression compared with controls (Fig. 6D), demonstrating a mechanism by which continuous exposure to Gem promotes the emergence of GemR mechanisms. RRM1 expression was decreased by BGJ398 alone after both 24 and 72 hours of exposure (Figs. 6, C and D), and the combination of Gem + BGJ398 further suppressed RRM1 expression after 24 hours of exposure, consistent with a delay in onset of RRM1-mediated GemR. By 72 hours of continuous

TABLE 2
Parameters estimated in the basic cell death model of Figs. 1 and 3

Parameter (Units)	Definition	Estimate	CV%	Confidence Interval (95%)
k_g (h^{-1})	Growth rate constant	0.059	3.2	0.055–0.062
R_0 ($\times 10^5$)	Initial seeding cell number	1.14	10.2	1.11–1.66
R_{ss} ($\times 10^7$)	Cell number at steady state	1.26	3.4	1.17–1.34
K_{max_Gem} (h^{-1})	Maximal cell kill rate constant for gemcitabine	0.054	11.7	0.042–0.067
KC_{50_Gem} (nM)	Gemcitabine concentration for half K_{max_GEM}	9.15	7.8	7.72–10.57
$1/\tau_{Gem}$ (h^{-1})	Mean transit time for gemcitabine cell kill signal	0.151	16.7	0.100–0.201
γ_{Gem}	Hill coefficient for gemcitabine	3.03	12.6	2.27–3.80
K_{max_BGJ} (h^{-1})	Maximal cell kill rate constant for BGJ398	0.058	24.3	0.030–0.086
KC_{50_BGJ} (μ M)	BGJ398 concentration for half K_{max_BGJ}	3.079	35.3	0.905–5.253
$1/\tau_{BGJ}$ (h^{-1})	Mean transit time for BGJ398 cell kill signal	0.114	10.8	0.089–0.139
γ_{BGJ}	Hill coefficient for BGJ398	1.31	26.4	0.617–1.999
Ψ_{death}	Interaction parameter	0.798	5.8	0.706–0.890

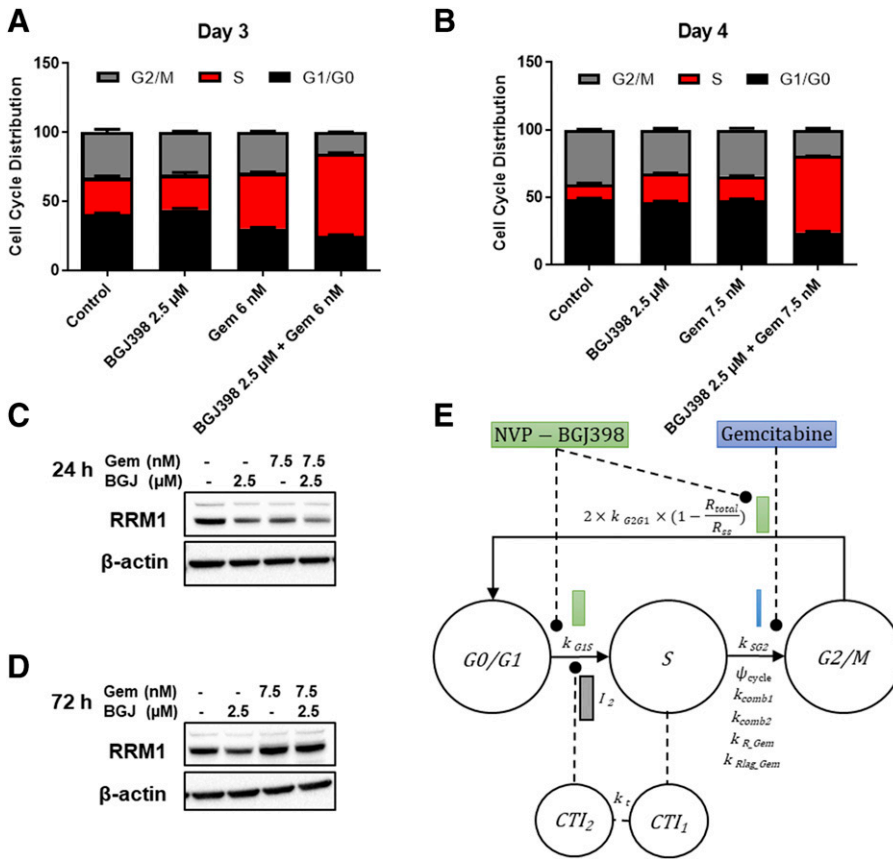


Fig. 6. Model schematic and cell cycle progression effects of combined gemcitabine and BGJ398. (A and B) Representative cell cycle distribution after exposure to vehicle, BGJ398 (2.5 μ M), Gem (6, 7.5 nM), and combined Gem + BGJ398 for (A) 72 hours and (B) 96 hours in MIAPaCa-2 cells. (C and D) Western blots of RRM1 and a β -actin loading control in MIAPaCa-2 cells treated with indicated concentrations of vehicle, BGJ398, Gem, alone and combination for (C) 24 hours and (D) 72 hours. (E) Schematic of the mechanism-based cell cycle progression model for combined Gem and BGJ398. The k_{comb1} and k_{comb2} parameters are used to describe the time delay of GemR onset and decreased magnitude of GemR. The drug interaction parameter ψ_{cycle} was used to describe the additional mechanisms by which BGJ398 sensitizes cells to Gem. Data shown are mean \pm S.D.

exposure of Gem + BGJ398, RRM1 was upregulated beyond control levels (Figs. 6, C and D), indicating the temporal limits of GemR delay by BGJ398.

To capture these data in the combined model of Fig. 6E, the lag time for onset of GemR and resumption of S-phase progression was extended proportional to the BGJ398 concentration (eq. 27), using the expression $(1 - k_{comb2} \cdot C_{BGJ})$ multiplied by k_{R_Gem} to describe the effect of BGJ398 to decrease the rate constants for GemR induction (eq. 28). The estimated coefficients for the attenuated GemR rate constants k_{comb1} and k_{comb2} were 9.65×10^{-3} and 3.92×10^{-2} (Table 3), consistent with a hypothesized prolongation of delay in GemR onset and decreased magnitude of GemR mediated by BGJ398. Because additional mechanisms may underlie the delayed onset of GemR, such as alterations in transporter activity (Namba et al., 2015; Zheng et al., 2015), DNA repair mechanisms (Crul et al., 2003; Akita et al., 2009), and apoptotic pathway activation (Beaujouin and Liaudet-Coopman, 2008), a cell cycle drug interaction term ψ_{cycle} was incorporated on the IC₅₀ of the Gem + BGJ398 combination (eqs. 29 and 30) to represent mechanisms not incorporated explicitly in the model. The model fitted the cell data well (Fig. 4), and the estimated ψ_{cycle} was 0.647 (CI: 0.6467–0.6473), suggesting the drug combination exerts overall synergistic effects in inhibiting cell cycle progression.

Effects of Single and Combined Drugs on Gem Transport. Receptor tyrosine kinase inhibitors such as those inhibiting the EGF and vascular endothelial growth factor (VEGF) receptors can block Gem transporter hENT1, which constitutes another pathway to GemR and a reduction in

Gem cytotoxicity (Damaraju et al., 2014). To investigate the potential effects of BGJ398 on Gem transporter hENT1, MIAPaCa-2 cells were treated with high concentrations of BGJ398 and Gem, alone and combined. BGJ398, Gem, or combination treatment did not change hENT1 expression (Supplemental Fig. 4A), indicating that transporter-mediated cellular Gem accumulation was not affected by FGFRi treatment, and that synergism of Gem + BGJ398 likely results predominantly from their pharmacological interactions at RRM1 induction and delay of the emergence of GemR (Figs. 6, C and D).

Effects of Single and Combined Drugs on PDAC Tumor Progression. Given the lack of experimental in vivo data for BGJ398 exposure in PDAC tumors, findings from the cell cycle progression modeling of drug interactions were employed in the design of a dosing regimen to test whether the Gem + BGJ398 combination would show efficacy in PDAC tumor models. The model parameter k_{Rlag_Gem} represents the minimal duration of BGJ398 exposure required to overcome GemR when combined with Gem. The magnitude of T_{Rlag_Gem} , calculated by fitting all data simultaneously (Supplemental Table 2), suggested that the onset of GemR in vitro is on the order of 61.5–69.2 hours, and that for BGJ398 to overcome GemR and reduce cell number, prolonged exposure of >61.5–69.2 hours would be required. Based upon the 13-hour half-life reported for BGJ398 in murine tumors (Guagnano et al., 2011), and the fact that most small molecule drugs achieve steady-state within four to five half-lives, BGJ398 exposure in tumors would be expected to reach steady-state in 52–65 hours after oral administration.

According to this rationale and the data available, we designed a treatment strategy that could potentially provide

TABLE 3
Parameters estimated in the mechanism-based cell cycle model in Figs. 4 and 5

Parameters for Unperturbed Cells (Units)	Definition	Estimate	CV%	Confidence Interval (95%)
k_{G1S} (h^{-1})	Transition rate between G0/G1 and S compartments	0.305	0.3	0.304–0.307
k_{SG2} (h^{-1})	Transition rate between S and G2/M compartments	0.1373	0.01	0.1373–0.1374
k_{G2G1} (h^{-1})	Transition rate between G2/M and G0/G1 compartments	0.1362	0.02	0.1361–0.1362
$G0/G1I_0$ (10^4 cells)	Number of cells in G0/G1 phase at initial seeding	2.76	3.7	2.56–2.97
S_0 (10^4 cells)	Number of cells in S phase at initial seeding	1.16	1.8	1.12–1.20
$G2/M_0$ (10^5 cells)	Number of cells in G2/M phase at seeding	24.5	0.3	24.4–24.6
R_s (10^4 cells)	Cell number at steady state	1580	0.05	1578–1581
K_r (h^{-1})	Transition rate constant between contact inhibition compartments (CTI ₁ and CTI ₂)	6.73×10^{-3}	0.5	6.67×10^{-3} - 6.81×10^{-3}
χ	Hill coefficient for CTI ₂ compartment	1 (fixed)		1 (fixed)
I_{max_CTI}	Maximal inhibitory effect for contact inhibition	1 (fixed)		1 (fixed)
χ_{CTI}	Hill coefficient of contact inhibition term I ₂	1 (fixed)		1 (fixed)
IT_{50} (h)	Time to half-maximal contact inhibition	56.6	0.7	55.8–57.4
Parameters for Gemcitabine-Treated Cells (Units)				
	Definition	Estimate	CV%	Confidence Interval (95%)
$I_{max_Gem_S}$	Maximal gemcitabine-induced S-phase cell cycle arrest	1 (fixed)		1 (fixed)
IC_{50_Gem} (nM)	Gemcitabine IC ₅₀ for cell cycle arrest effects	5.57	0.03	5.57–5.58
χ_{Gem}	Hill coefficient for gemcitabine S-phase arrest	1.98	0.02	1.98–1.99
k_{R_Gem} (h^{-1})	First-order rate constant of recovery to normal cell cycle progression after Gem treatment	0.182	0.08	0.181–0.182
k_{Rlag_Gem} (h^{-1})	First-order rate constant for delay of gemcitabine resistance onset	79.1	0.03	79.0–79.1
Parameters for BGJ398-Treated Cells (Units)				
	Definition	Estimate	CV%	Confidence Interval (95%)
$I_{max_BGJ_G1G2}$	Maximal BGJ398-induced G1 and G2/M phase cell cycle arrest	1 (fixed)		1 (fixed)
IC_{50_BGJ} (nM)	BGJ398 IC ₅₀ for cell cycle arrest	3605	0.02	3604–3606
χ_{BGJ}	Hill coefficient for BGJ398-induced G0/G1 and G2/M phase cell cycle arrest	1.808	0.01	1.808–1.809
Parameters for Cells Treated with Combination (Units)				
	Definition	Estimate	CV%	Confidence Interval (95%)
ψ_{cycle}	Interaction term for cell cycle arrest	0.647	0.02	0.6467–0.6473
k_{comb1} (nM^{-1})	First-order rate constant for prolongation of delay in onset of gemcitabine resistance induced by BGJ398	9.65×10^{-5}	0.2	9.61×10^{-5} - 9.69×10^{-5}
k_{comb2} (nM^{-1})	First-order rate constant for decreased magnitude of gemcitabine resistance mediated by BGJ398	3.92×10^{-4}	0.01	3.917×10^{-4} - 3.919×10^{-4}

≥ 120 hours of BGJ398 exposure in tumors, which modeling had suggested would be required to suppress GemR. BGJ398 was administered by mouth for 5 days to SCID mice bearing subcutaneous MIA PaCa-2 tumors, followed by a 2-day drug holiday before the next cycle. Gem was administered intraperitoneally on the 1st and 4th day of BGJ398 treatment. Strikingly, neither single-agent Gem (10 or 30 mg/kg) nor BGJ398 (15 or 45 mg/kg) significantly slowed mean tumor progression (Fig. 7A), and tumors progressed to a protocol volume limit within two to three cycles of treatment (Figs. 7, B–E). In contrast, the rate of tumor progression was reduced in all groups treated with combined Gem + BGJ398. By the end of the third treatment cycle, all mice treated with vehicle or BGJ398 alone, and more than 60% mice in the Gem groups, had been removed from study because of tumor progression. At the completion of the experiment on day 21, all groups treated with combined Gem + BGJ398 had significantly lower mean tumor volumes ($P \leq 0.05$) than any of the control- or single-agent treatment groups (Fig. 7A), and more than 80% mice in the Gem + BGJ398 combination groups remained well below the tumor volume threshold limit (Figs. 7, G–I).

Discussion

In most patients with pancreatic cancer, onset of GemR is rapid, and the lack of effective therapies contributes to the high mortality of PDAC. More effective therapeutic strategies and integration of new targeted agents with standard-of-care regimens are needed urgently. Numerous factors contributing to GemR have been reported, including multiple mutations in key signaling pathways (Amrutkar and Gladhaug, 2017), Gem metabolism by intratumor bacteria (Geller et al., 2017), downregulation of the Gem uptake transporter hENT1 (Nakano et al., 2007; Namba et al., 2015), upregulation of RRM1 and mesenchymal biomarkers (Nakahira et al., 2007; Wang et al., 2009), and both poor tumor vascularization and stromal amplification that together constitute a physical barrier to drug delivery (Li et al., 2012). Emerging data demonstrate that aberrant FGFR signaling also contributes to PDAC cell proliferation, survival, and invasion (Coleman et al., 2014; Kang et al., 2019), yet the therapeutic utility of FGFRi has not been elucidated in PDAC. Here, we demonstrate that inhibition of FGFR signaling by a pan-FGFR inhibitor enhanced Gem efficacy in vitro and in vivo. Under the treatment conditions employed in vitro, hENT1 expression was unchanged after BGJ398 treatment of MIA PaCa-2 cells, and thus, it is likely that the synergism results between the two drugs predominately from pharmacological interactions rather than from transporter-mediated pharmacokinetic interactions.

Based upon experimental data, two pharmacodynamic models were developed to assess Gem + BGJ398 interactions systematically. A basic cell proliferation/death model was employed to describe temporal changes in PDAC cell number during treatment with the drugs alone and combined, and the model was able to describe both cytostatic and cytotoxic drug effects. By comparing the threshold concentration required for cytotoxic effects with the experimental concentrations employed (Miao et al., 2016a), the effects of these two drugs could be well differentiated. A mechanism-based pharmacodynamic model of cell cycle distribution was also developed to characterize the nature of drug interaction with combined Gem + BGJ398.

The predominant effect of both Gem and BGJ398 was to stall cell cycle progression. Exposure to single-agent Gem initially led to an accumulation of cells in S phase, as observed previously for PANC-1 PDAC cells (Zhu et al., 2015). S-phase arrest diminished at later times, suggesting the onset of DNA damage repair, a GemR mechanism (Ewald et al., 2007). After 72 hours of Gem exposure, we found that RRM1 expression increased, suggesting the onset of at least one GemR mechanism. Treatment with BGJ398 alone resulted in cell accumulation in G₀/G₁ and G₂/M phases. When combined with Gem, the effect was prolonged, and enhanced S-phase arrest was observed after 72 and 96 hours of exposure. Early in exposure, BGJ398 treatment also increased the downregulation of RRM1, which also reduces GemR. These observations suggest that BGJ398 sensitizes cells to Gem by delaying the onset of GemR mechanisms and decreasing their magnitude.

Several model parameters have important implications for preclinical therapeutic studies and molecular mechanisms. First, consistent with these individual observations of reduced GemR described above, the drug interaction terms ψ_{death} and ψ_{cycle} in the pharmacodynamic models describe quantitatively an overall synergistic inhibition of Gem + BGJ398 on PDAC cell proliferation and cell cycle progression over an extended treatment period. These drug interaction terms, derived from the in vitro culture system, support the possibility of supra-additive inhibition of tumor progression by Gem + BGJ398 regimens in vivo. Second, the biologic meaning of these two ψ values differs. In the basic cell death model, ψ_{death} enables the model to account for interactions at the level of both cytostatic and cytotoxic effects, whereas in the cell cycle model, ψ_{cycle} quantifies drug interactions that increase the sensitivity of cell cycle progression to Gem inhibition. Notably, the estimated values of these drug interaction terms from the two models were similar, suggesting that the interaction occurs primarily in the suppression of cell cycle progression. Additional mechanisms underlying synergy may emerge, such as increased aneuploidy, because potential mechanisms at higher Gem concentrations ($>15 \mu\text{M}$) were not included in the cell cycle model. We hypothesize that aneuploidy induced by Gem represents an intermediate state between cell cycle arrest and apoptosis, consistent with observations that cell stress inducers, such as the adenosine kinase/adenosine inhibitor aminoimidazole carboxamide ribonucleotide and the heat shock protein 90 (HSP90) inhibitor 17-AAG, trigger apoptosis to a greater extent in highly aneuploid cells (Manchado and Malumbres, 2011; Tang et al., 2011). Future extension of the model to incorporate these more complex effects could capture additional mechanisms of drug interaction at higher concentrations, but simplifying assumptions in the present model appear justified at concentrations close to the Gem IC₅₀. Third, consideration of both GemR mechanisms and pharmacokinetics contributed to the design of an effective combination treatment regimen. The GemR-associated parameters k_{Rlag_Gem} and T_{Rlag_Gem} suggested that a minimal duration of BGJ398 exposure (>61.5 – 69.2 hours) would be required to overcome GemR when combined with Gem. Based upon the limited pharmacokinetic data available for BGJ398 in tumors (Guagnano et al., 2011), we surmised that 52–65 hours would be required to reach tumor steady-state. Therefore, a weekly regimen of two Gem treatments overlaid upon a 5-day daily BGJ398 treatment window was selected for initial proof-of-concept studies, and a Gem-resistant PDAC tumor model was

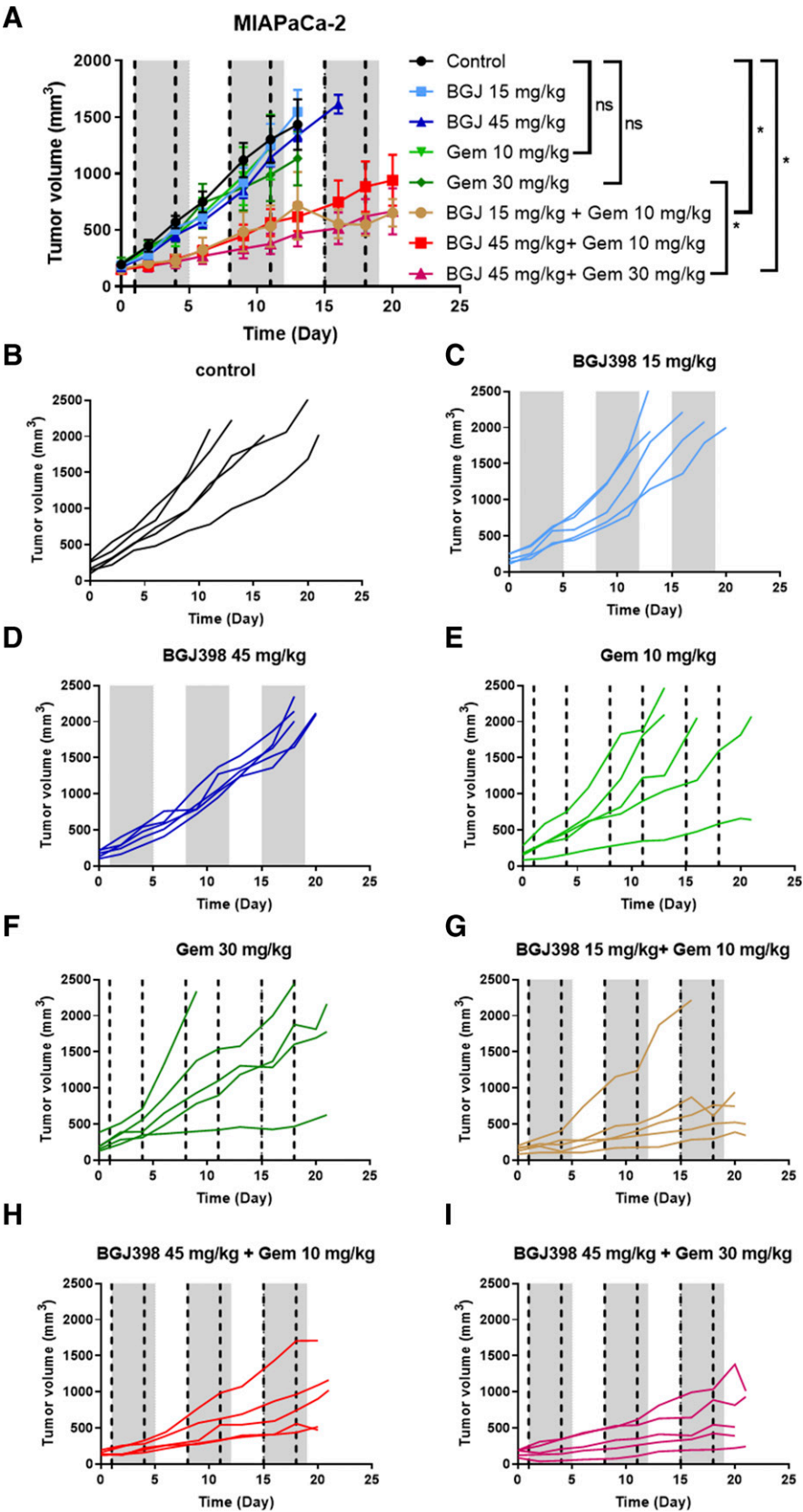


Fig. 7. Effects of treatment on tumor progression in a PDAC model. SCID mice bearing subcutaneous MIAPaCa-2 tumors were treated with vehicle or the indicated doses of BGJ398, Gem, or Gem + BGJ398 for three cycles ($n = 5/\text{group}$). (A) Censored tumor volumes and body weight were measured throughout the treatment period; data for the mean tumor volume is no longer plotted when the second of two animals reached the protocol tumor volume limit of 2000 mm^3 . Vertical dashed lines indicate days of intraperitoneal administration of Gem (10 or 30 mg/kg). Gray shaded bands indicate 5-day periods of daily oral dosing with BGJ398 (15 or 45 mg/kg). Data shown are mean \pm S.E.M.; $P \leq 0.05$, *; ns, not significant. The decrease in tumor volume on day 17 in the group Gem (10 mg/kg) + BGJ398 (15 mg/kg) resulted from the removal of one animal because of tumor growth to protocol limits (Fig. 7G). No animals were removed from study in any group because of body weight loss or declining body condition. The experiment was completed on day 21 after the initiation of dosing, when more than 60% of the control- and single-agent mice had been removed from study. (B–I) Individual tumor progression data for each animal in the treatment groups.

employed to explore the efficacy of combined Gem + BGJ398. Although neither agent alone elicited statistically significant responses, despite the 3-fold range of concentrations administered, the combination regimen suppressed tumor progression markedly, without perceptible toxicity. Thus, parameter values derived from the in vitro models provided a starting point to devise an exploratory dosing regimen that demonstrated superior efficacy. Further investigation of additional treatment regimens is under way in a set of diverse patient-derived PDAC xenograft models that capture a broad range of GemR phenotypes. Of interest is an apparent lack of a dose-response relationship in the two combined Gem + BGJ398 treatment groups; tripling the dose of BGJ398 and Gem did not appear to prolong inhibition of tumor volume progression. However, the study was neither intended nor powered to identify a dose-response relationship. Further analysis of in vivo drug interaction and response mechanisms remains to be defined, and will require extension of the models developed here to include tumor microenvironment effects, such as the complex autocrine and paracrine signaling interactions that occur in vivo, as well as the influence of multiple cell types within the tumor that respond to FGF signaling or FGFR inhibition. Nonetheless, this initial in vivo evaluation of combined Gem + BGJ398 on a Gem-resistant PDAC model that revealed the combination prolonged survival significantly and advances the rationale, generated from in vitro findings of supra-additive effects of combined Gem + BGJ298 upon PDAC cell cycle progression and proliferation, that FGFRi treatment represents a promising approach to sensitize PDAC tumors to Gem therapy.

The potential therapeutic impact of integration of FGFRi into the two standard-of-care regimens for PDAC, Gem + nab-paclitaxel and FOLFIRINOX, remains to be determined. Work in progress indicates that Gem + BGJ398 is at least equivalent, and possibly superior to Gem + nab-paclitaxel in inhibiting progression of a patient-derived xenograft tumor model, and addition of BGJ398 to the standard-of-care Gem + nab-paclitaxel combination mediates a significant increase in efficacy (unpublished data). These results are consistent with recent reports that paclitaxel prolongs Gem-mediated inhibition of S-phase progression (Passacantilli et al., 2018), and suggest that BGJ398 may cooperate mechanistically to increase efficacy of Gem + nab-paclitaxel. Studies investigating in vitro interactions in the four-drug FOLFIRINOX regimen (Zoetemelk et al., 2020) report both additivity and antagonism in promoting cell death, with which our in vitro studies are consistent (unpublished data). Preliminary results in vitro suggest that combining BGJ398 with irinotecan, oxaliplatin, or 5-FU decreases cell growth statistically (unpublished data), but the nature of the pharmacodynamic interaction has not been analyzed. Thus FGFRi interactions with the FOLFIRINOX drugs merit thorough investigation.

In conclusion, quantitative pharmacodynamic modeling and analysis of experimental data that capture the interactions of a pan-FGFRi with Gem, a standard-of-care agent in PDAC, suggest two important mechanisms by which the FGFRi could improve outcomes with Gem-based therapy. The first is that the two drugs synergize in the delay of cell cycle progression that primes PDAC cells for eventual apoptosis. The second is that the FGFRi sensitizes cells to Gem by reversing GemR or delaying its onset, thereby augmenting Gem-based efficacy significantly. The Gem + BGJ398 combination also exerts significant efficacy in vivo

PDAC models. Further preclinical investigation into broader integration of FGFR inhibitors in standard-of-care PDAC therapy could increase clinical responses, and is supported by these studies.

Acknowledgments

We thank Drs. Xin Miao and Xu Zhu for helpful suggestions in model development.

Authorship Contributions

Participated in research design: Lin, Ma, Straubinger.

Conducted experiments: Lin, Qian.

Performed data analysis: Lin, Qian, Jusko, Mager, Straubinger.

Wrote or contributed to the writing of the manuscript: Lin, Jusko, Mager, Straubinger.

References

- Ait-Oudhia S, Straubinger RM, and Mager DE (2013) Systems pharmacological analysis of paclitaxel-mediated tumor priming that enhances nanocarrier deposition and efficacy. *J Pharmacol Exp Ther* **344**:103–112.
- Akita H, Zheng Z, Takeda Y, Kim C, Kittaka N, Kobayashi S, Marubashi S, Take-masa I, Nagano H, Dono K, et al. (2009) Significance of RRM1 and ERCC1 expression in resectable pancreatic adenocarcinoma. *Oncogene* **28**:2903–2909.
- Amrutkar M and Gladhaug IP (2017) Pancreatic Cancer Chemoresistance to gemcitabine. *Cancers (Basel)* **9**:157.
- Ariens EJ, Van Rossum JM, and Simonis AM (1957) Affinity, intrinsic activity and drug interactions. *Pharmacol Rev* **9**:218–236.
- Babina IS and Turner NC (2017) Advances and challenges in targeting FGFR signalling in cancer. *Nat Rev Cancer* **17**:318–332.
- Battaglia MA and Parker RS (2011) Pharmacokinetic/pharmacodynamic modelling of intracellular gemcitabine triphosphate accumulation: translating in vitro to in vivo. *IET Syst Biol* **5**:34.
- Beaujourn M and Liaudet-Coopman E (2008) Cathepsin D overexpressed by cancer cells can enhance apoptosis-dependent chemo-sensitivity independently of its catalytic activity. *Adv Exp Med Biol* **617**:453–461.
- Binenbaum Y, Na'ara S, and Gil Z (2015) Gemcitabine resistance in pancreatic ductal adenocarcinoma. *Drug Resist Updat* **23**:55–68.
- Cappella P, Tomasoni D, Faretti M, Lupi M, Montalenti F, Viale F, Banzato F, D'Incalci M, and Ubezio P (2001) Cell cycle effects of gemcitabine. *Int J Cancer* **93**:401–408.
- Chakraborty A and Jusko WJ (2002) Pharmacodynamic interaction of recombinant human interleukin-10 and prednisolone using in vitro whole blood lymphocyte proliferation. *J Pharm Sci* **91**:1334–1342.
- Coleman SJ, Chioni AM, Ghallab M, Anderson RK, Lemoine NR, Kocher HM, and Grose RP (2014) Nuclear translocation of FGFR1 and FGF2 in pancreatic stellate cells facilitates pancreatic cancer cell invasion. *EMBO Mol Med* **6**:467–481.
- Crul M, van Waardenburg RC, Bocxe S, van Eijndhoven MA, Pluim D, Beijnen JH, and Schellens JH (2003) DNA repair mechanisms involved in gemcitabine cytotoxicity and in the interaction between gemcitabine and cisplatin. *Biochem Pharmacol* **65**:275–282.
- Curtis MJ, Alexander S, Cirino G, Docherty JR, George CH, Gienbycz MA, Hoyer D, Insel PA, Izzo AA, Ji Y, et al. (2018) Experimental design and analysis and their reporting II: updated and simplified guidance for authors and peer reviewers. *Br J Pharmacol* **175**:987–993.
- Damaraju VL, Scriver T, Mowles D, Kuzma M, Ryan AJ, Cass CE, and Sawyer MB (2014) Erlotinib, gefitinib, and vandetanib inhibit human nucleoside transporters and protect cancer cells from gemcitabine cytotoxicity. *Clin Cancer Res* **20**:176–186.
- Di Marco M, Di Cicilia R, Macchini M, Nobili E, Vecchiarelli S, Brandi G, and Biasco G (2010) Metastatic pancreatic cancer: is gemcitabine still the best standard treatment? (Review). *Oncol Rep* **23**:1183–1192.
- Dimou A, Syrigos KN, and Saif MW (2012) Overcoming the stromal barrier: technologies to optimize drug delivery in pancreatic cancer. *Ther Adv Med Oncol* **4**:271–279.
- Ewald B, Sampath D, and Plunkett W (2007) H2AX phosphorylation marks gemcitabine-induced stalled replication forks and their collapse upon S-phase checkpoint abrogation. *Mol Cancer Ther* **6**:1239–1248.
- Geller LT, Barzily-Rokni M, Danino T, Jonas OH, Shental N, Nejman D, Gavert N, Zhang Y, Cooper ZA, Shee K, et al. (2017) Potential role of intratumor bacteria in mediating tumor resistance to the chemotherapeutic drug gemcitabine. *Science* **357**:1156–1160.
- Greenhalf W, Ghanesh P, Neoptolemos JP, Palmer DH, Cox TF, Lamb RF, Garner E, Campbell F, Mackey JR, Costello E, et al.; European Study Group for Pancreatic Cancer (2014) Pancreatic cancer hENT1 expression and survival from gemcitabine in patients from the ESPAC-3 trial. *J Natl Cancer Inst* **106**:dj347.
- Guagnano V, Furet P, Spanka C, Bordas V, Le Douget M, Stamm C, Brueggen J, Jensen MR, Schnell C, Schmid H, et al. (2011) Discovery of 3-(2,6-dichloro-3,5-dimethoxy-phenyl)-1-[6-[4-(4-ethyl-piperazin-1-yl)-phenylamino]-pyrimidin-4-yl]-1-methyl-urea (NVP-BGJ398), a potent and selective inhibitor of the fibroblast growth factor receptor family of receptor tyrosine kinase. *J Med Chem* **54**:7066–7083.
- Guagnano V, Kauffmann A, Wöhrle S, Stamm C, Ito M, Barys L, Pornon A, Yao Y, Li F, Zhang Y, et al. (2012) FGFR genetic alterations predict for sensitivity to NVP-BGJ398, a selective pan-FGFR inhibitor. *Cancer Discov* **2**:1118–1133.

- Hamed SS, Straubinger RM, and Jusko WJ (2013) Pharmacodynamic modeling of cell cycle and apoptotic effects of gemcitabine on pancreatic adenocarcinoma cells. *Cancer Chemother Pharmacol* **72**:553–563.
- Jordheim LP, Sève P, Trédan O, and Dumontet C (2011) The ribonucleotide reductase large subunit (RRM1) as a predictive factor in patients with cancer. *Lancet Oncol* **12**:693–702.
- Kang X, Lin Z, Xu M, Pan J, and Wang ZW (2019) Deciphering role of FGFR signalling pathway in pancreatic cancer. *Cell Prolif* **52**:e12605.
- Karlsson MO, Anehall T, Friberg LE, Henningsson A, Kloft C, Sandström M, and Xie R (2005) Pharmacokinetic/pharmacodynamic modelling in oncological drug development. *Basic Clin Pharmacol Toxicol* **96**:206–211.
- Katopodis O, Souglakos J, Stathopoulos E, Christopoulou A, Kontopodis E, Kotsakis A, Kalbakis K, Kentepozidis N, Polyzos A, Hatzidaki D, et al. (2014) Frontline treatment with gemcitabine, oxaliplatin and erlotinib for the treatment of advanced or metastatic pancreatic cancer: a multicenter phase II study of the Hellenic Oncology Research Group (HORG). *Cancer Chemother Pharmacol* **74**:333–340.
- Lehnen NC, von Massenhausen A, Kalthoff H, Zhou H, Glowka T, Schütte U, Höller T, Riesner K, Boehm D, Merkelbach-Bruse S, et al. (2013) Fibroblast growth factor receptor 1 gene amplification in pancreatic ductal adenocarcinoma. *Histopathology* **63**:157–166.
- Li X, Ma Q, Xu Q, Duan W, Lei J, and Wu E (2012) Targeting the cancer-stroma interaction: a potential approach for pancreatic cancer treatment. *Curr Pharm Des* **18**:2404–2415.
- Louvet C, Labianca R, Hammel P, Lledo G, Zampino MG, André T, Zaniboni A, Ducreux M, Aitini E, Taieb J, et al.; GERCOR; GISCAD (2005) Gemcitabine in combination with oxaliplatin compared with gemcitabine alone in locally advanced or metastatic pancreatic cancer: results of a GERCOR and GISCAD phase III trial. *J Clin Oncol* **23**:3509–3516.
- Manchado E and Malumbres M (2011) Targeting aneuploidy for cancer therapy. *Cell* **144**:465–466.
- Miao X, Koch G, Ait-Oudhia S, Straubinger RM, and Jusko WJ (2016a) Pharmacodynamic modeling of cell cycle effects for gemcitabine and trabectedin combinations in pancreatic cancer cells. *Front Pharmacol* **7**:421.
- Miao X, Koch G, Straubinger RM, and Jusko WJ (2016b) Pharmacodynamic modeling of combined chemotherapeutic effects predicts synergistic activity of gemcitabine and trabectedin in pancreatic cancer cells. *Cancer Chemother Pharmacol* **77**:181–193.
- Molins EAG and Jusko WJ (2018) Assessment of three-drug combination pharmacodynamic interactions in pancreatic cancer cells. *AAPS J* **20**:80.
- Nakahira S, Nakamori S, Tsujie M, Takahashi Y, Okami J, Yoshioka S, Yamasaki M, Marubashi S, Takemasa I, Miyamoto A, et al. (2007) Involvement of ribonucleotide reductase M1 subunit overexpression in gemcitabine resistance of human pancreatic cancer. *Int J Cancer* **120**:1355–1363.
- Nakano Y, Tanno S, Koizumi K, Nishikawa T, Nakamura K, Minoguchi M, Izawa T, Mizukami Y, Okumura T, and Kohgo Y (2007) Gemcitabine chemoresistance and molecular markers associated with gemcitabine transport and metabolism in human pancreatic cancer cells. *Br J Cancer* **96**:457–463.
- Namba T, Kodama R, Moritomo S, Hoshino T, and Mizushima T (2015) Zidovudine, an anti-viral drug, resensitizes gemcitabine-resistant pancreatic cancer cells to gemcitabine by inhibition of the Akt-GSK3 β -Snail pathway. *Cell Death Dis* **6**:e1795.
- Niu J, Straubinger RM, and Mager DE (2019) Pharmacodynamic drug-drug interactions. *Clin Pharmacol Ther* **105**:1395–1406.
- Nogova L, Sequist LV, Perez Garcia JM, Andre F, Delord JP, Hidalgo M, Schellens JH, Cassier PA, Camidge DR, Schuler M, et al. (2017) Evaluation of BGJ398, a fibroblast growth factor receptor 1–3 kinase inhibitor, in patients with advanced solid tumors harboring genetic alterations in fibroblast growth factor receptors: results of a global phase I, dose-escalation and dose-expansion study. *J Clin Oncol* **35**:157–165.
- Passacantilli I, Panzeri V, Terracciano F, Delle Fave G, Sette C, and Capurso G (2018) Co-treatment with gemcitabine and nab-paclitaxel exerts additive effects on pancreatic cancer cell death. *Oncol Rep* **39**:1984–1990.
- Pawaskar DK, Straubinger RM, Fetterly GJ, Ma WW, and Jusko WJ (2013) Interactions of everolimus and sorafenib in pancreatic cancer cells. *AAPS J* **15**:78–84.
- Plunkett W, Huang P, Xu YZ, Heinemann V, Grunewald R, and Gandhi V (1995) Gemcitabine: metabolism, mechanisms of action, and self-potential. *Semin Oncol* **22**(Suppl 11):3–10.
- Rauchwerger DR, Firby PS, Hedley DW, and Moore MJ (2000) Equilibrative-sensitive nucleoside transporter and its role in gemcitabine sensitivity. *Cancer Res* **60**:6075–6079.
- Sarkar FH, Li Y, Wang Z, and Kong D (2009) Pancreatic cancer stem cells and EMT in drug resistance and metastasis. *Minerva Chir* **64**:489–500.
- Siegel RL, Miller KD, and Jemal A (2017) Cancer statistics, 2017. *CA Cancer J Clin* **67**:7–30.
- Song S, Wientjes MG, Gan Y, and Au JL (2000) Fibroblast growth factors: an epigenetic mechanism of broad spectrum resistance to anticancer drugs. *Proc Natl Acad Sci USA* **97**:8658–8663.
- Strömberg T, Ekman S, Girnita L, Dimberg LY, Larsson O, Axelsson M, Lennartsson J, Hellman U, Carlson K, Osterborg A, et al. (2006) IGF-1 receptor tyrosine kinase inhibition by the cyclolignan PPP induces G2/M-phase accumulation and apoptosis in multiple myeloma cells. *Blood* **107**:669–678.
- Tang YC, Williams BR, Siegel JJ, and Amon A (2011) Identification of aneuploidy-selective antiproliferation compounds. *Cell* **144**:499–512.
- Thoenissen NH, Iwanski GB, Doan NB, Okamoto R, Lin P, Abbassi S, Song JH, Yin D, Toh M, Xie WD, et al. (2009) Cucurbitacin B induces apoptosis by inhibition of the JAK/STAT pathway and potentiates antiproliferative effects of gemcitabine on pancreatic cancer cells. *Cancer Res* **69**:5876–5884.
- Thota R, Pauff JM, and Berlin JD (2014) Treatment of metastatic pancreatic adenocarcinoma: a review. *Oncology (Williston Park)* **28**:70–74.
- Tomlinson DC, Baxter EW, Loadman PM, Hull MA, and Knowles MA (2012) FGFR1-induced epithelial to mesenchymal transition through MAPK/PLC γ /COX-2-mediated mechanisms. *PLoS One* **7**:e38972.
- Vaccaro V, Sperduti I, and Milella M (2011) FOLFIRINOX versus gemcitabine for metastatic pancreatic cancer. *N Engl J Med* **365**:768–769, author reply 769.
- Van Cutsem E, Bang YJ, Mansoor W, Petty RD, Chao Y, Cunningham D, Ferry DR, Smith NR, Frewer P, Ratnayake J, et al. (2017) A randomized, open-label study of the efficacy and safety of AZD4547 monotherapy versus paclitaxel for the treatment of advanced gastric adenocarcinoma with FGFR2 polysomy or gene amplification. *Ann Oncol* **28**:1316–1324.
- Vena F, Hartley JA, and Hochhauser D (2016) The MEK1/2 inhibitor pimasertib enhances gemcitabine efficacy-response. *Clin Cancer Res* **22**:2595.
- Von Hoff DD, Ervin T, Arena FP, Chiorean EG, Infante J, Moore M, Seay T, Tjuland SA, Ma WW, Saleh MN, et al. (2013) Increased survival in pancreatic cancer with nab-paclitaxel plus gemcitabine. *N Engl J Med* **369**:1691–1703.
- Wagner M, Lopez ME, Cahn M, and Korc M (1998) Suppression of fibroblast growth factor receptor signaling inhibits pancreatic cancer growth in vitro and in vivo. *Gastroenterology* **114**:798–807.
- Wang Z, Li Y, Kong D, Banerjee S, Ahmad A, Azmi AS, Ali S, Abbruzzese JL, Gallick GE, and Sarkar FH (2009) Acquisition of epithelial-mesenchymal transition phenotype of gemcitabine-resistant pancreatic cancer cells is linked with activation of the notch signaling pathway. *Cancer Res* **69**:2400–2407.
- Wu F, Buckley S, Bui KC, Yee A, Wu HY, Liu J, and Warburton D (1996) Cell cycle arrest in G0/G1 phase by contact inhibition and TGF β -1 in mink Mv1Lu lung epithelial cells. *Am J Physiol* **270**:L879–L888.
- Zheng X, Carstens JL, Kim J, Scheible M, Kaye J, Sugimoto H, Wu CC, LeBleu VS, and Kalluri R (2015) Epithelial-to-mesenchymal transition is dispensable for metastasis but induces chemoresistance in pancreatic cancer. *Nature* **527**:525–530.
- Zhou W, Huang A, Zhang Y, Lin Q, Guo W, You Z, Yi Z, Liu M, and Chen Y (2015) Design and optimization of hybrid of 2,4-diaminopyrimidine and arylthiazole scaffold as anticancer cell proliferation and migration agents. *Eur J Med Chem* **96**:269–280.
- Zhu X, Straubinger RM, and Jusko WJ (2015) Mechanism-based mathematical modeling of combined gemcitabine and birinapant in pancreatic cancer cells. *J Pharmacokinet Pharmacodyn* **42**:477–496.
- Zhu XF, Liu ZC, Xie BF, Li ZM, Feng GK, Yang D, and Zeng YX (2001) EGFR tyrosine kinase inhibitor AG1478 inhibits cell proliferation and arrests cell cycle in nasopharyngeal carcinoma cells. *Cancer Lett* **169**:27–32.
- Zoetemelk M, Ramzy GM, Rausch M, and Nowak-Sliwinska P (2020) Drug-drug interactions of irinotecan, 5-fluorouracil, folinic acid and oxaliplatin and its activity in colorectal carcinoma treatment. *Molecules* **25**:2614.

Address correspondence to: Dr. Robert M. Straubinger, The Department of Pharmaceutical Sciences, 319 Pharmacy Bldg., University at Buffalo, State University of New York, Buffalo, NY 14214. E-mail: rms@Buffalo.edu